UNIVERSITAT POLITÈCNICA
DE CATALUNYA

Identification of a system with dry friction

Claudiu Iurian, Fayçal Ikhouane, José Rodellar, Robert Griñó

IOC-DT-P-2005-20
Setembre 2005

Institut d'Organització i Control
de Sistemes Industrials

Contents

Part 1

The State of the Art in Friction Modeling for Systems Identification

1.1 INTRODUCTION

Friction is a complex nonlinear phenomenon. A great deal is known about friction in specific circumstances, but not in the general case, if there is such a thing. There is still much to be learned about its nature and how it changes under different circumstances, and how it can be predicted and controlled. Indeed, it is difficult to find a process, in nature or industry, that is entirely free of friction [1]. Examples of frictional effects in everyday life are, without a doubt, endless.

What is the definition of friction? Before anything else, we must say that the term friction is used more as a descriptive convenience rather than as a rigorous definition of friction phenomenon. The term friction comes from the Latin verb *fricare*, that is, to rub. The word tribology (Greek word for the study of rubbing), however, includes not only friction but also lubrication and wear. So, tribology is the science of the mechanisms of friction, lubrication, and wear of interaction bodies that are in relative motion. Tribology addresses and answers questions such as the true contact area, the relationships between friction, material properties and lubricating processes, wear mechanisms, and so on. In [2] is presented a timeline of the scientific study of friction starting with Leonardo Da Vinci (1452) giving the 1994 state of the art in friction for control purposes. Until recently, in tribology frictional dynamics has not been a focus [2]. Nevertheless, for the control engineer the *dynamics* of friction is of greatest interest; and here, lately, the control literature has become a major developer.

We will focus only on just a group of frictional phenomena: static and dynamic friction between solid bodies, friction modelling, and compensation methods for machines with friction.
Usually friction is not wanted, so a great deal has been done to reduce it by design, or by control. Friction introduces significant limitations to achieving good performance in controlled mechanical systems. In this respect, a widely used principle of friction control is model-based friction compensation which is utilized to apply a force or torque command equal and opposite in sign to the instantaneous friction force. An accurate friction model is needed for this purpose. Thus, various mathematical relationships have been developed to determine the influence of friction on machine behavior. Due to the fact that friction is such a common phenomenon, when feedback control methods are applied to machines and bodies in motion, friction appears invariably among the forces of motion [2] and which, oftentimes, cannot be simply ignored.

The number of friction models proposed in literature is huge, see [2] for a complete literature survey, and can be subdivided with respect to their detail in describing surface contact properties occurring on a microscopic and macroscopic level. In the past decade major effort and contributions [3], [4], [5] are made in the development of friction models, suitable for analysis and controller synthesis, which have relatively limited complexity but a relevant similarity to practically observed friction phenomena.

1.2 STATIC FICTION MODELS

Various mathematical models have been proposed in the literature that describe the important friction phenomena observed. Most of them are still used now, which model is preferred now depends on the purpose of it, but the model that accurately describes all the observed phenomena is in general to be preferred. Besides the question of effectiveness

also the model efficiency, e.g., the required computational resources in terms of time, can be of importance when for instance the model will be used in simulation studies. Due to the complexity of the physical mechanisms underlying friction, most models are of an empirical nature. Furthermore, a distinction was made between *static* and *dynamic* models depending on the inclusion of frictional memory. For static friction models, this frictional memory is not take into account, whereas for dynamic friction models this memory behavior is described with additional dynamics between velocity and the friction force.

The observed friction phenomena during the early days of scientific study of friction, Amontons in [6], then Coulomb in [7], and then others, have led to models of Coulomb, viscous, static friction (stiction), and their possible combinations, which are often referred to as *classical models of friction*. The Stribeck model, which models the Stribeck effect [8], can also be classified nowadays as belonging to this set of models. Four possible combinations are shown below.

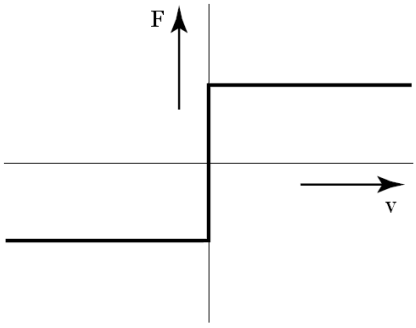

(a) Coulomb

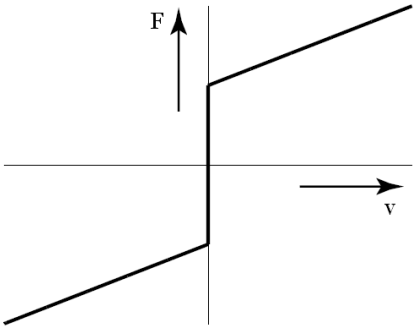

(b) Coulomb + viscous

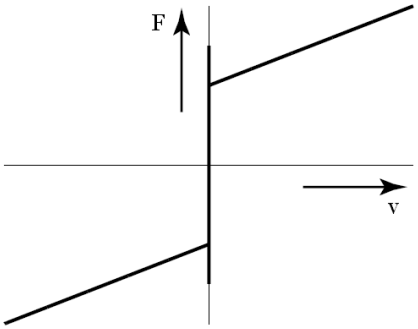

(c) Coulomb + viscous + stiction

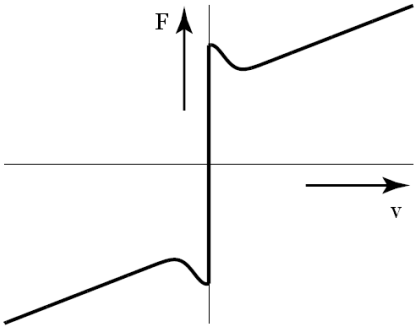

(d) Coulomb + viscous + Stribeck effect

The static friction models are those that give the friction forces a function of velocity. These models only describe the steady-state behavior between velocity and friction force. One drawback of the above models is discontinuity at zero velocity that allows the friction rate to take on an infinite number of possible values. The discontinuity does not reflect the real friction behavior in a good way and causes errors or even instability in the algorithms used to compensate friction.

1.2.1 Coulomb Friction

Independent of the area of contact, the Coulomb friction always opposes relative motion and is proportional to the normal force of contact. The Coulomb friction is the friction phenomenon that is only dependent of the direction of the velocity, not of the magnitude of the velocity. It is modelled as a static map between velocity and friction force that depends on the sign of the velocity.

$$F = F_C \, sgn(v)$$

where $F_C = \mu |f_n|$, μ being the coefficient for friction and f_n the normal force.

Coulomb friction is called also *kinetic friction* because it defines friction for non-zero velocities. For zero velocities

the above Coulomb friction depends upon the *signum* function definition. A common use of the switching function is

$$sgn(v) = \begin{cases} +1 & \forall \quad v > 0 \\ 0 & \forall \quad v = 0 \\ -1 & \forall \quad v < 0 \end{cases}$$

A question that immediately arises is with Coulomb friction and which is very important because can create instability in the algorithms that depend on the true zero velocity to compensate friction is: *When precisely the velocity reaches and crosses the zero level?* In fact, this is the fundamental problem with all *classical models of friction* they are not causal, i.e., the discontinuity at zero velocity permits friction to take an infinite number of values [9].

1.2.2 Viscous Friction

Viscous friction results from the viscous behavior of a fluid lubricant layer between two rubbing surfaces. As shown in above, viscous friction is represented as a linear function of velocity.

$$F = F_v v$$

Viscous friction is the friction component that is proportional to velocity and goes to zero at zero velocity.

1.2.3 Stiction

Experimentally has been observed that friction force at rest is higher than the kinetic force or Coulomb friction. If the system is in sticking an externally applied force is need that is equal or greater than the stiction force to put the body in motion, i.e. in slipping. This has been studied intensely in the 1950s, see the study of Rabinowicz [10] about the nature of the static and kinetic coefficients of friction. Static friction (stiction) is the force required to initiate motion from rest. Typically, the magnitude of static friction is greater than the magnitude of Coulomb friction which can lead to intermittent motion known as stick-slip motion.

Stiction is assumed to be independent of the velocity, however varies as a function of the dwell-time when sticking and the rate of increase of the applied force. Thus, friction at rest cannot be described as a function of only velocity. Instead, it has to be captured in the model an external force F_e as in the following description.

$$F = \begin{cases} F_e & \text{if} \quad v = 0 \quad \text{and} \quad |F_e| < F_s \\ F_S \, sgn(F_e) & \text{if} \quad v = 0 \quad \text{and} \quad |F_e| \geq F_s \end{cases}$$

1.2.4 Stribeck Effect

Stribeck effect is the friction phenomenon that arises from the use of fluid lubrication and gives rise to decreasing friction with increasing velocity at low velocity. For low velocities the friction force decreases with increasing velocity. Stribeck effect is needed to correctly predict initial conditions leading to stick-slip motion.

Stribeck curve [8] is a continuous drop in the friction force for small velocities, which originates from the transition of boundary lubrication to full fluid lubrication through partial fluid lubrication [2]. The Stribeck effect could not be ignored for most of the cases and had been introduced and used extensively into the new frictional models developed.

1.2.5 Continuous zero-velocity crossing model

The discontinuity of friction at zero velocity can lead to unwanted consequences such as (1) non-uniqueness of the solutions to the equations of motion for the system [2] which can occur in real friction and (2) numerical problems if such a model is used in simulation like numerical chatter. Precautions have to be taken when numerically integrating a system model that includes discontinuities as introduced by the classical friction models. One approach to overcome

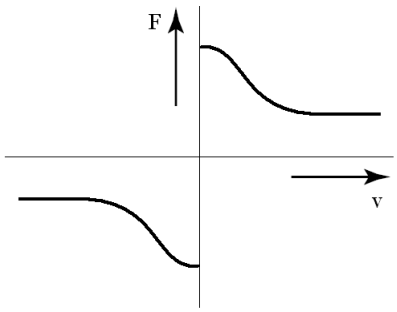

(e) Stribeck curve of steady-state friction force

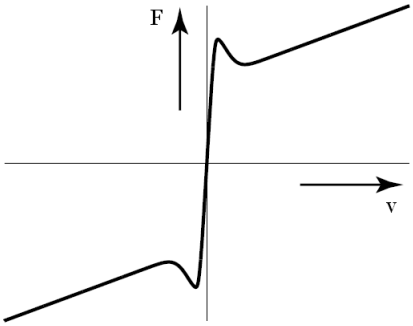

(f) Continuous zero-velocity crossing model

the discontinuity is approximating or smoothing the map by a curve with finite slope [11] as depicted in the figure below

Nonetheless, a very steep slope around zero velocity can result in very short integration time steps which slows down simulation. Moreover, the body connected to the frictional contact surface will accelerate even if the external forces on the body are less than the peak static friction force Fs and therefore these alternate friction models will not provide true stiction.

1.2.6 A more general static model

A more general model than the classical models of friction is given in [12] and it covers Coulomb, viscous, stiction, and Stribeck friction.

$$F = \begin{cases} F(v) & \text{if} \quad v \neq 0 \quad \text{and} \quad |F_e| < F_s \\ F_e & \text{if} \quad v = 0 \quad \text{and} \quad |F_e| < F_s \\ F_S\, sgn(F_e) & \text{otherwise} \end{cases}$$

where $F(v)$ is a nonlinear function, e.g., of the form

$$F(v) = F_C + (F_S - F_C)e^{-\left|\frac{v}{v_s}\right|^{\delta}} + F_v v$$

with v_s as the Stribeck velocity and δ as the form factor. Such kind of friction models have been used for quite a long time.

1.2.7 Karnopp Model

For control purposes, the main disadvantage when using a model such as the general model above, is the problem of detecting when exactly the velocity is zero. Karnopp in [13] developed a model to overcome the problems with zero

velocity detection and to avoid switching between different state equations for sticking and sliding. The model defines a zero velocity interval, $|v| < DV$. For velocities within this interval the internal state of the system the velocity may change and be non-zero but the output of the block is maintained at zero by a dead-zone.

The drawback with the model is that it is so strongly coupled with the rest of the system. The external force is an input to the model and this force is not always explicitly given. The model therefore has to be tailored for each configuration. Variations of the Karnopp model are widely used since they allow efficient simulations. Nevertheless, the zero velocity interval does not agree with real friction phenomenon and has not been used to extensively.

1.2.8 The seven parameter model

The seven parameter model is a friction model designed to include all relevant experimentally observed friction phenomena and was proposed by Armstrong in [2], [11]. It consists of two separate models: a stiction model and a sliding model. During stiction, friction is modelled as a stiff spring to account for presliding displacements.

$$F_f(x) = \sigma x$$

In sliding, the model is modelled as Coulomb + viscous + Stribeck effect with frictional memory:

$$F_f(\dot{x},t) = \left(F_c + F_v|\dot{x}| + F_s(\gamma,t_2)\frac{1}{1+\left(\frac{\dot{x}(t-\tau_L)}{\dot{x}_s}\right)^2} \right) sgn(\dot{x})$$

where

$$F_s(\gamma,t_2) = F_{s,a} + (F_{s,\infty} - F_{s,a})\frac{t_2}{t_2+\gamma}$$

describes the varying friction level at break-away.

The level of the stiction force F_s varies with the time at zero velocity t_2 (dwell time). A long dwell time means a high break-away force. The force $F_{s,a}$ is the magnitude of the Stribeck friction at the end of the previous sliding period; γ is an empirical parameter. The friction force for the sliding mode is equivalent to a static friction model where the velocity has been replaced with a delayed version and which has a time-dependent coefficient F_s [14]. The time delay τ_L models the desired frictional memory. When used in simulations some mechanism has to be employed to switch between the two modes for sliding and stiction. Also, the model states x and $\dot{x}$ have to be initialized appropriately every time a switch occurs. Although useful for analysis of stick-slip behavior [11], for simulation purposes the model seems to be less appropriate, see [15] where was performed a simulation study employing, amongst several other friction models, the seven parameter model.

1.3 FRICTION PHENOMENA

Experimentally has been shown that friction in control applications exhibits phenomena that cannot be modelled with a static friction model as above, such as presliding displacement, frictional lag, varying break-away force, and stick-slip motion. In studying friction there is a clear necessity of using dynamic friction models to take those phenomena into account and, thus, the following properties of a friction model are considered to be very important for the control of friction in mechanical systems.

1.3.1 Presliding Displacement

If a force is applied to two surfaces in contact a small displacement will always occur due to limited stiffness of contact asperities [8]. Friction force behaves like a spring (and that causes a displacement linear dependent on the applied force) if the externally applied force is less than the break-away force. Small motions in the elastic region in sticking are referred to as presliding displacement or the Dahl effect. Presliding displacement is a consequence of elastic deformation of the surface asperities where contact and sliding occur and it significantly influences friction forces during velocity reversal [11]. It is the compliance of presliding displacement that softens the hard nonlinearity of friction at zero velocity. Presliding displacement is needed to correctly predict small displacements while sticking (including velocity reversals).

Contrary to the predictions derived from the classical friction model, researchers including Courtney-Pratt and Eisner [16] and others have found experimentally that small relative displacements between two bodies in contact do occur when the applied relative tangential force is less than the static friction. Although the magnitude of this pre-sliding displacement is small, with sufficient gain, as in a robot with a fairly long link, small displacements at the rubbing surface can translate into significant displacements elsewhere in the mechanism. Further, the nature of pre-sliding displacements provides insight into a difficult part of the control problem, the transition between sticking and sliding. Courtney-Pratt and Eisner interpreted the pre-sliding phenomenon within the framework of the theory of asperity junction adhesion, asperity junctions being the load bearing interfaces between rubbing surfaces. Specifically, as the shear force at the contact surfaces increases, the asperity junctions deform elastically and then plastically. When the applied force finally reaches the stiction level, the asperity junctions break and sliding begins. Because of the plastic deformation, alternate increases and decreases in applied tangential force result in friction hysteresis loops. The pre-sliding displacement phenomenon is illustrated in figure below, which shows friction F as a function of displacement x based on experimental results.

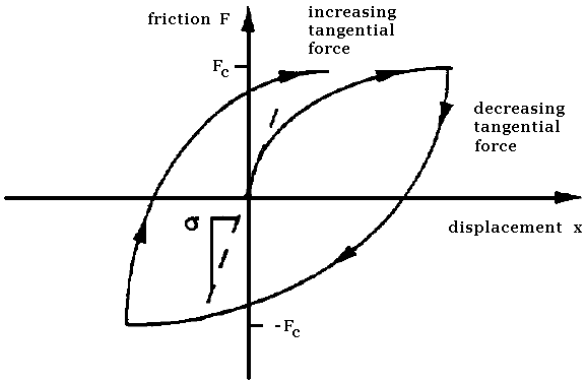

1.3.2 Frictional Lag

Frictional lag is the delay in the change of the friction force as function of a change in the velocity which may have a significant impact on dynamics as noted by Hess and Soom [17]. There is a hysteresis in the relationship between friction force and velocity. Namely, the friction force is lower for decreasing velocities than it is for increasing velocities. The width of the hysteresis loop increases with frequency and with higher rates of velocity changes [3].

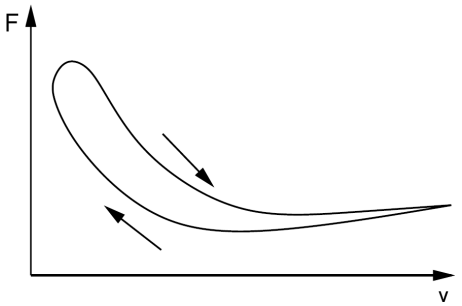

Frictional lag is a dynamic behavior that results in a larger friction force for increasing velocities than for decreasing velocities and becomes more apparent for large acceleration and/or deceleration [17].

We note the considerable empirical evidence that has become available indicating that friction does not respond instantaneously to a change in velocity. The primary work here is due to geophysicists who use stick-slip for earthquake-related predictions. Hess and Soom also found strong evidence of frictional lag, in their experiments on a flat steel button rubbing against a rotating steel disk. Frictional lag makes stick-slip instabilities less likely. Because a decrease in friction occurs slowly when velocity is increased, stiff systems will not experience stick-slip [11].

1.3.3 Varying Break-Away Force

The break-away force is the force required to overcome stiction and initiate motion and it has been intensely studied for the last several decades [2]. Varying break-away force or rising static friction (sometimes also called static friction level) is the dependence of the break-away force on the rate of increase of the applied force [16].

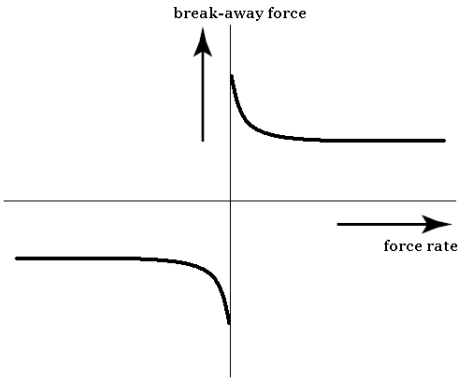

The dwell-time when sticking is always related to the rate of increase of the applied force and the effects cause by these two connected factors cannot be separated. Also, the break-away force can be interpreted in the control systems as the minimum open-loop force.

1.3.4 Stick-Slip Motion

Stick-slip motion manifests itself as repeated sequences of sticking between two surfaces with static friction followed by sliding or slipping of the two surfaces, for instance, when moving slowly, machines are likely to exhibit stick-slip motion [11]. Stick-slip is a phenomenon which happens when sliding one body over another under a steady pulling force and the sliding velocity fluctuates widely. These fluctuations consist of sticking where the motion stops and slipping where the bodies suddenly accelerate again. In most practical sliding systems, these fluctuations of the sliding velocity are considered a serious nuisance. Eliminating or reducing the amplitude of the fluctuations is usually necessary. Stick-slip motion is caused by the fact that friction is larger at rest than during motion. When the applied force reaches the break-away force the body starts to slide and friction decreases rapidly due to the Stribeck effect.

For the servo-mechanism control problem, stick-slip can diminish control accuracy. The stick-slip limit cycling can be avoided if damping and stiffness are sufficiently high.

1.3.5 Time-dependent, position dependent, and direction-dependent friction

Time-dependent friction - From practical experiments can be seen that friction changes with time [1]. These changes of friction with time are due to such things as loss of lubricant, deformation of the surface material, change in temperature due to generated heat and accumulation of wear debris, and the like.

Position-dependent friction - Friction exhibits also a dependence on the positioning of a system. This has been experimentally observed and is well known by a lot of tribology researchers. This position-dependency is caused by spatial inhomogeneities [1] in the transmission of the system due to contact geometry and loading which varies as a function of position. As the load varies, the normal force between the sliding surfaces varies, causing a varying friction.

Direction-dependent friction - Again, experimentally, has been found the friction to be dependent on the direction of the motion of a system. Different Coulomb and viscous friction levels in the left and right directions of a single, linear motion have been observed experimentally on many occasions. This may be due to anisotropies in material or material geometry.

1.4 DYNAMIC FICTION MODELS

One of the major disadvantage of the discussed static friction models is the limited richness of the models, which will result in inaccurate friction models for certain regions of interest, such as presliding displacement in the stiction regime or frictional lag for the sliding regime. For the analysis of friction related problems or controller synthesis these phenomena may be of importance, which motivated control researchers to make a creative effort in this direction.

The seven parameter model and similar static models try to capture the dynamics of friction by introducing time dependency or a time delay. A better alternative approach is the use of dynamic models, which are also often referred to as state variable models. In its general form state variable models were introduced by geophysicists to study stick-slip phenomena. Interest in these phenomena stems from the hypothesis that earthquakes are stick-slip events, in which the earth's tectonic plates in succession stick and slip . The idea is to introduce extra state variables (or internal states) that determine the level of friction in addition to velocity. The evolution in time of the state variables is governed by a set of differential equations. Often the introduced state variables can be given a physical interpretation, which depends on the friction mechanism that the friction model is supposed to describe. Over the past decades a few friction models belonging to this class have been proposed, i.e., in the late 1960's the Dahl model [18], but only recently interest seems to have increased especially within the control community where several dynamic friction models have been proposed in the 1990's by Haessig et al. [4], Dupont et al. [19], Canudas de Wit et al. [3] and Bliman et al. [5]. The research path which starts with the Dahl model will be discussed in more detail, because it resulted in the nowadays widely used dynamic LuGre friction model [3]. To describe presliding displacements, i.e., elastic and plastic deformations of the asperity junctions before macroscopic sliding, Dahl thought of exploiting the stress-strain curve of two surfaces under contact known from solid mechanics. Dahl showed how the stress-strain curve can be transformed into a force-displacement curve.

1.4.1 Dahl Model

Dahl model is a generalization of the ordinary Coulomb friction, that is, the steady-state version of Dahl model is Coulomb friction. Dahl [18] started with the following relation for the stress-strain curve.

$$\frac{dF}{dt} = \frac{\partial F}{\partial t} + \frac{\partial F}{\partial x}\frac{dx}{dt}$$

Then he made the assumption that $\frac{dF}{dx}$ does not depend on the variable t:

$$\frac{dF}{dt} = \frac{\partial F}{\partial x}\frac{dx}{dt}$$

$$\frac{dF}{dt} = \frac{dF}{dx}\frac{dx}{dt} = \frac{dF}{dx}v$$

It can be noted that with $\frac{dF}{dx} = k$, where k is a positive constant, by integration the expression can be written as $F = kx$ which is a linear spring model. The general Dahl model is written as:

$$\frac{dF}{dx} = \sigma_0 \left|1 - \frac{F}{F_C} sgn\, v\right|^i sgn\left(1 - \frac{F}{F_C} sgn\, v\right)$$

or

$$\frac{dF}{dt} = \sigma_0 \left|1 - \frac{F}{F_C} sgn\, v\right|^i sgn\left(1 - \frac{F}{F_C} sgn\, v\right) v$$

With $i = 1$ we get the simplified Dahl model which is used much more.

$$\frac{dF}{dx} = \sigma_0 \left(1 - \frac{F}{F_C} sgn\, v\right)$$

or

$$\frac{dF}{dt} = \sigma_0 \left(1 - \frac{F}{F_C} sgn\, v\right)\frac{dx}{dt} = \sigma_0 \left(1 - \frac{F}{F_C} sgn\, v\right)v$$

that is

$$\frac{dF}{dt} = \sigma_0 v - \sigma_0 \frac{F}{F_C} sgn(v) v$$

Introducing $F = \sigma_0 z$, which means also that $\dot{z} = \frac{\dot{F}}{\sigma_0}$, we get

$$\begin{aligned} \dot{z} &= v - \frac{\sigma_0 z}{F_C} |v| \\ F &= \sigma_0 z \end{aligned}$$

in steady state Dahl model simplifies to

$$z = \frac{F_C}{\sigma_0} sgn\ v$$

$$F = F_C sgn\ v$$

that is, the Coulomb friction model.

Dahl model does not capture Stribeck effect (which is a rate dependent phenomenon) nor does it capture stiction.

It can be observed also that LuGre model reduces to Dahl model if $g(v) = \frac{F_C}{\sigma_0}$ and $\sigma_1 = \sigma_2 = 0$.

1.4.2 The Bristle Model

The contact of two rough technical surfaces the external forces lead to elastic and plastic deformations of the contacting asperities. The bristle model captures the randomness of friction that originates from the random distribution of asperities on a surface and was introduced by Haessig and Friedland [4]. They assume friction between two contact surfaces to be caused by a large number of interacting bristles.

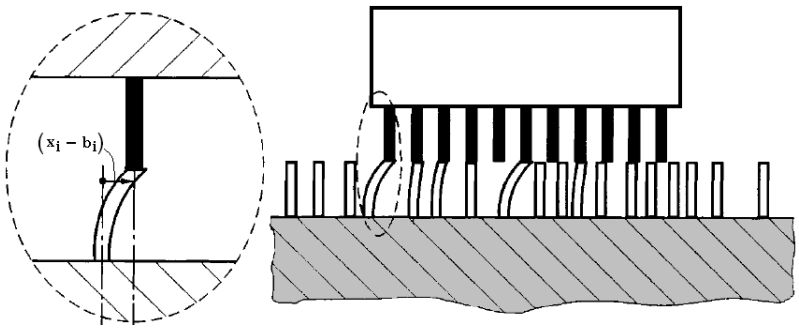

A connected bristle acts as a spring and when the strain $|x_i - b_i|$ of a certain bristle exceeds a certain level the connection is broken and a new connection with a random strain is established. Friction is made a function of velocity by further assuming that the number of bristles depends on the relative velocity of the opposing surfaces. The friction force is the sum total of the separate spring forces and is

$$F = \sum_{i=1}^{N} \sigma_0 (x_i - b_i)$$

where

N - the number of bristles
σ_0 - the stiffness of the bristles
x_i - the relative position of the bristles
b_i - the location where a connection takes place

The model captures the random nature of friction which depends on the number of bristles chosen, the greater the number the more complex the bristle model. This makes the model inefficient as far as the complexity of the algorithms is concerned. Numerically, the bristle model is highly ineffective and is therefore normally not be used in simulations. The merits of this model are found in the interpretation of friction as interacting bristles and the real-life random behavior that it reproduces.

1.4.3 The Reset Integrator Model

In the same paper Haessig et al. [4] introduces a more workable and numerically more efficient model for simulation purposes named the reset integrator model. This models the bonding effect during stiction by a single position variable named presliding displacement z, the local randomness of friction being modelled by averaging the stochastic properties of the different bristle connections.

This model captures the dynamic effects of friction using an integrator with a reset action to distinguish between the two cases *sticking* and *slipping*. When a characteristic presliding distance z_1 is reached macroscopic sliding starts and the model changes from the sticking mode to the slipping mode. In must observed as was already the case for the Karnopp model and the seven parameter model, the friction model consists of two different models which are coupled by a switching variable. The position variable z viewed as a state variable, and its dynamics is given by:

$$\dot{z} = \begin{cases} 0 & \text{if} \quad \dot{x} > 0 \quad \text{and} \quad z \geq z_1 \\ 0 & \text{if} \quad \dot{x} < 0 \quad \text{and} \quad z \leq -z_1 \\ \dot{x} & \text{otherwise} \end{cases}$$

The friction force can be only in two modes, either stiction or sliding:

$$F = \begin{cases} \sigma_0(\dot{x})(1+a)z + \sigma_1 \dot{z} & |z| < z_1 \\ \sigma_0(\dot{x})z_1 & |z| \geq z_1 \end{cases}$$

where $\sigma_1 \dot{z}$ is an supplementary damping term introduced physical realism by having damped oscillations during the sticking mode and introduces the viscous friction effects during presliding. The stiffness $\sigma_0(\dot{x})$ is an arbitrary function of velocity and the coefficient a is added to give a higher level for stiction. During stiction, the friction force cancels the driving force through spring-damper system. The reset integrator model is discontinuous in the state variable z due to switching from stiction to sliding and numerical problems may arise for very large damping values or spring stiffness.

1.4.4 Models for lubricated contacts

The friction interfaces in most engineering applications are lubricated. Friction interfaces in machineries and real applications are lubricated and for this reason friction models have been derived in the literature using hydrodynamics, for instance the viscous friction, but other lubricated models were also developed. Harnoy and Friedland [20] propesed a model based on the hydrodynamics of a lubricated journal bearing. The model stresses the dynamics of the friction force. The eccentricity e of the bearing is an important variable in determining the friction force. A simple model is given by

$$F = K_1(\varepsilon - \varepsilon_{tr})^2 \Delta + \frac{K_2}{\sqrt{1-\varepsilon^2}} v$$

It consists of two terms, first term is due to the shearing of the asperity contacts and the second term is due to the viscosity of the lubricant and has five parameters.

$$\Delta = \begin{cases} 1 & \text{if} \quad \varepsilon > \varepsilon_{tr} \\ 0 & \text{otherwise} \end{cases}$$

The function Δ implies that for small eccentricities there is no friction due to asperity contacts. The eccentricity is given by a fourth-order differential equation, which determines the pressure distribution in the lubricant. The model from the start requires initial values when switching between slipping and sticking occurs.

1.4.5 Bliman-Sorine Model

Another dynamic friction model inspired by the Dahl model is the Bliman-Sorine friction model [5]. This second order linear dynamic friction model connects a fast and a slow Dahl model in parallel, where the fast model has the highest steady-state friction and the force from the slow model is subtracted from the fast model, which results in a stiction peak. However, comparison studies [21], [22], [14] revealed that the dynamic LuGre model is beneficial with respect to the ability to model rate dependent friction phenomena, such as varying breakaway force and frictional lag. Moreover, the model order of the Bliman-Sorine model is higher than for the LuGre model and the damping properties during stiction is numerically more efficient for the Lugre model. Hence, the Bliman-Sorine friction model will not be used further.

Bliman-Sorine model generalizes Dahl model to obtain the Stribeck effect. Bliman and Sorine replaced the time variable t by a space variable s through the transformation

$$ds = |v(t)|dt$$

or the integral form

$$s = \int_0^t |v(\tau)|d\tau$$

The variable s is a space variable defined as the *absolute relative displacement* of the bodies in contact since the last change of velocity sign. By applying the above transformation to the simplified Dahl model we get

$$\frac{dF}{dt} = \sigma_0 v - \sigma_0 \frac{F}{F_C} sgn(v)v$$

$$\frac{dF}{ds}|v(t)| = \sigma_0 v - \sigma_0 \frac{F}{F_C} sgn(v)v$$

$$\frac{dF}{ds} = -\sigma_0 \frac{F}{F_C} + \sigma_0 sgn(v)$$

which is a linear first-order system if $sgn(v)$ is regarded as an input.

Bliman and Sorine replaced the equation above by a second-order model

$$\frac{d^2F}{ds^2} + 2\xi\omega\frac{dF}{ds} + \omega^2 F = \omega^2 F_C sgn(v)$$

in order to model stiction force as an overshoot in response to sign changes in the velocity. This model gives only a spatially transient Stribeck effect after a change of the direction of motion and the Stribeck effect is not present in the steady-state relation between velocity and friction force.

Bliman-Sorine model is rate independent.

1.4.6 LuGre Model

A model that is in line with the considerations of the Dahl model and also employs the idea of an averaged characteristic presliding displacement, as introduced by Heassig et al. [4], has been proposed by Canudas de Wit et al. [3], where it is presented as the LuGre model. It combines the Dahl model with arbitrary steady-state characteristics such as the Stribeck effect. However, the interpretation of the internal state is that of the bristle model, i.e., friction is visualized as forces produced by bending bristles behaving like springs, but instead of modelling the random behavior of friction it is based on the average behavior of the bristles. LuGre model is rate dependent.

In the LuGre model the friction force during stiction is modelled as the average force applied by a set of elastic springs under a tangential microscopic displacement. An interpretation of these elastic springs can be given under the assumption that the two moving surfaces are in contact by a large number of bristles with a certain stiffness which can be represented as in the figure below.

Bristle stiffness and microscopic damping are introduced to model the average bristle displacement.

$$\dot{z} = v - \frac{\sigma_0}{g(v)} z\,|v| \tag{1}$$

$$g(v) = F_C + (F_S - F_C)\, e^{-(v/v_s)^2} \tag{2}$$

$$F = \sigma_0 z + \sigma_1 \dot{z} + \sigma_2 v \tag{3}$$

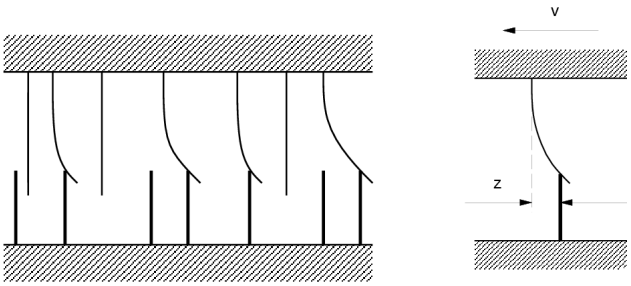

where

$v(t)$	is the relative velocity of the bodies in contact.
z	is the average bristle deflection; z is the internal state of the model.
σ_0	is the stiffness of the bristles.
σ_1	is the microscopic damping.
σ_2	is the viscous friction coefficient.
$g(v)$	is the function that models the Stribeck effect, i.e., the Stribeck curve for steady-state velocities.
$f(v)$	is the viscous friction.
F_C	is the Coulomb friction level.
F_S	is the stiction level.
F	is the tangential friction force, the output of the model.
v_s	is the Stribeck velocity and determines how $g(v)$ varies within its bounds $F_c \leq g(v) \leq F_s - F_c$.
$\sigma_2 v$	is the viscous friction (important only for higher velocities).

LuGre model description is characterized by six parameters: $\sigma_0, \sigma_1, \sigma_2, F_C, F_S$, and v_s.
σ_0, σ_1 are the *dynamic parameters*.
F_C, F_S, v_s, and σ_2 are the *static parameters*.

For the same reason as with the reset integrator model an extra damping term is included and viscous friction is represented by $\sigma_2 v$. The Stribeck effect is reproduced by assuming that the average deflection of the bristles at steady-state motion, and therefore the friction force, decreases with increasing velocity. Thus, neglecting for a moment viscous friction, at steady-state the friction force is given by

$$F = \sigma_0 z = g(v)\, sgn(v)$$

The LuGre friction model is a special case of the model and is denoted as the standard parametrization, which is due to linear viscous friction and a constant bristle microscopic damping parameter σ_1 [14]. This standard parametrization can be restrictive with respect to the desired passivity property of friction as shown by Barabanov et al. [23] who present necessary conditions so that the passivity property to hold for the LuGre model. The conditions are expressed in terms of a simple algebraic inequality involving the parameters of the model. A velocity dependent parametrization of the bristle damping might result in a model which is dissipative. If the damping coefficient 1 decreases for increasing velocity, a dissipative model is obtained, which is physically motivated by the change of the damping characteristics as velocity increases, due to more lubricant being forced into the interface of the two contact surfaces.

In turn, Lugre model has been subjected to several criticisms by Swevers et al. [24], mainly focusing on the relation imposed in the LuGre model between the friction force during presliding and the state variable of the model. Swevers et al. showed by experiments that the relation is more complicated, and is characterized by hysteresis behavior with nonlocal memory. They also modified accordingly the LuGre model into the Leuven model. These findings were also confirmed in [25]. Later, the stack mechanism used to implement the hysteresis behavior (quite cumbersome to be implemented in real-time systems) has been replaced by the more efficient. Another criticism to the LuGre model has been recently raised by Dupont et al. [26], who underline a nonphysical drift phenomenon, arising when the applied force is characterized by small vibrations, well below the static friction limit.

1.4.7 Leuven Model

The integrated friction model by Swevers et al. in [24] called the Leuven model is a more elaborated friction model than the LuGre model proposed by Canudas de Wit et al. [3]. Leuven model structure allows accurate modelling both in the presliding and the sliding regimes without the use of a switching function. The model incorporates a hysteresis function with nonlocal memory and arbitrary transition curves. This model can account accurately for experimentally obtained friction characteristics: Stribeck effect in sliding, friction lag, varying break-away, stick-slip behavior and, hysteretic behavior in presliding. This last property cannot be modeled with the LuGre model.

Leuven model also consists of two equations: a friction force equation and a nonlinear state equation. It uses a state variable z which can be seen as the average deflection of the asperity junctions.

$$\frac{dz}{dt} = v\left(1 - sgn\left(\frac{F_d(z)}{s(v)-F_b}\right)\left|\frac{F_d(z)}{s(v)-F_b}\right|^n\right)$$

$$F_f = F_h(z) + \sigma_1\frac{dz}{dt} + \sigma_2 v$$

where

v is the current velocity
n is a coefficient used to shape the transition curves
$s(v)$ is a function that models the constant velocity behavior

$$s(v) = sgn(v)\left(F_C + (F_s - F_C)\,e^{-\left(\frac{|v|}{V_s}\right)^{\delta}}\right)$$

$F_h(z)$ is the hysteresis force, i.e., the part of the friction force exhibiting hysteresis behavior with state variable z as input. The hysteresis force is a static nonlinearity with a nonlocal memory. The implementation of the hysteresis force is made of two parts

$$F_h(z) = F_b + F_d(z)$$

with F_b being the beginning of a transition curve at velocity reversal and $F_d(z)$ the transition curve active at a certain time.

Leuven Model includes the friction properties of the LuGre model and a more accurate modeling of the presliding regime using a hysteresis function with nonlocal memory. Leuven model has been improved in [27] by overcoming the detected problem of a discontinuity in the friction force upon closing a hysteresis loop and by proposing a more appropriate implementation of the hysteresis force based on the general Maxwell slip model which can eliminate the problem of stack overflow noted in [24] for the Leuven model implementation.

1.5 CONCLUSIONS

We have reviewed the mathematical models of friction used in controls literature starting from the simplest to the most complex, each of them trying in one way or another to capture the complex friction phenomena. It must be stressed that LuGre model is today one of the most used in the literature. LuGre model exhibits a rich behavior in terms of observed friction phenomena and in particular is able to model: stiction, the Stribeck effect, frictional lag or hysteresis, and stick-slip transitions. However, some of the practically observed hysteresis related phenomena can not be predicted accurately by the LuGre model as noted by Olsson et al. [14] and Swevers et al. [24]. The latter proposes an extension of the LuGre model to approach these hysteresis problems. The notion of stiction is re-addressed by Dupont et al. [19], who discusses the difference between stiction and presliding displacement. In their analysis both the dynamic Dahl and LuGre friction models are considered to possess presliding displacement but no stiction. A new elasto-plastic state variable friction model is proposed which models both stiction and presliding displacement. However, the proposed Leuven model by Swevers et al. [24] is more complex than the standard parametrization of the LuGre model due to the use of a hybrid hysteresis model and therefore more difficult to be used for control design and analysis. On the other hand, the elasto-plastic state variable friction model proposed by Dupont et al. [19] is mainly based on simulation studies and the presented ideas are not yet confirmed experimentally. Hence, the standard parametrization of the LuGre model is still most wildly used nowadays.

All these experimentally observed phenomena and their modelation are necessary to fully understand the problems present in controlled mechanical systems with friction, since a motion system faces one or more of the above described frictional stages for each task performed. Moreover, the simplest friction model combining all these properties has to contain extra dynamics for the modelling of varying static friction and hysteresis due to frictional lag and should at the same time be nonlinear to capture the Stribeck curve. However, for the analysis of controlled mechanical systems, simplification of the friction model is often necessary due to the limited applicability of the used analysis tools. On the other hand, some friction induced phenomena can successfully be described with less complex friction models, which is desirable from a conceptual point of view and is also an important research issue. The estimation of the model parameters is important for obtaining quantitatively accurate friction models, which can be used as a mathematical representation of the friction. In general, it is not possible to measure the friction force directly and therefore the identification of friction in a mechanical system is far from trivial. Since the friction force can not be observed directly, experiments for the identification procedure are performed by sensing quantities that are influenced indirectly by the friction force, such as displacements, velocities or acceleration of the mass connected to the frictional contact surface. To estimate the model parameters, often extended with parameters to describe other dynamics in the system, such as mass and stiffness, different dedicated and time-consuming experiments must to be conducted. Each experiment must be designed to visualize one of the friction phenomena as described above by excluding other dynamics in the system. However, the time-varying nature of friction due to wear and exogenous variables such as changing load or operating temperatures might limit the applicability of an estimated friction model considerably. At a macroscopic level friction forces vary in time due to microscopic effects such as deformation of contact surfaces, accumulation of wear particles or changes in the properties of the lubricant. Since these influences are hard to measure it is also difficult to model these time varying phenomena. Hence, the estimated friction model is expected to capture at best an averaged behavior of the actual friction over time. Validation of the friction model with its estimated parameters can either focus on the ability of the identified model to predict the friction characteristics of interest or on the closed-loop performance when the identified friction model is incorporated in the controller design. Typical errors caused by friction in control loops are steady-state errors in position regulation, tracking lags, and limit cycles. The models can be validated in an open-loop or closed-loop setting and results might be improved, if desirable, in an iterative procedure, by choosing a more complex friction model.

Part 2

Summary of the Work Done

2.1 M220 - THE EQUATIONS OF MOTION

For the purpose of studying friction phenomena in all detail our investigation group CoDAlab from UPC Barcelona has purchased an industrial emulator made by ECP Systems, see [28], which will be referred to from now on as M220. This machine is a solid tool and testbed used primarily for experimentation in systems identification and control. M220 consists of a drive inertia and a load inertia, namely, it has a motor connected to a first smaller disk or "drive inertia" which in turn is connected to an idler pulley by an inelastic belt whose shaft is connected to the second larger disk or "load inertia".

The main advantages offered by M220 are: 1) it can be used for studying the nonlinear dry friction phenomena that occur in mechanical systems, and 2) it provides accurate and reliable data by means of high resolution encoders controlled by a DSP controller and a specialized C-like software which interface with a PC.

2.1.1 Two-gear belt mechanism

Let us consider the *two-gear belt mechanism* as shown below.

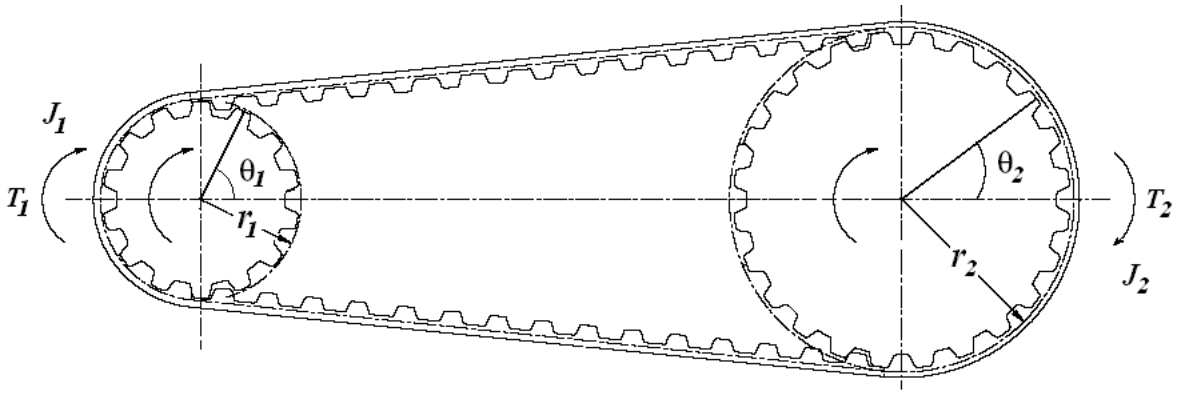

We have:

θ_1 is the angular position of the *driving gear* (motored).
θ_2 is the angular position of the *driven gear* (load).
r_1 is the *radius* of the driving gear.
r_2 is the *radius* of the driven gear.
Gear ratio is the number of turns the *driving gear* (motored - or *first* gear) does per one single turn of the *driven gear* (load - or *second* gear).
$n_g = \frac{r_2}{r_1}$ is the **gear ratio**, and because $n_g > 1$ is called *speed reducer*.
J_1 is the driving gear *inertia*.
J_2 is the driven gear *inertia*.

T_1 is the *torque* of the driving gear (generated by the driving motor).
T_2 is the *torque* of the driven gear (load torque).

Definition 1 **Inertia** is the resistance an object has relative to changes in velocity.

Definition 2 The **moment of inertia J** of a body is a measure of how hard it is to get it rotating about some axis. The moment **J** is to rotation as mass **m** is to translation. The larger the **J**, the more work required to get the object spinning, just as the larger the mass **m**, the more work required to get it moving in a straight line.

Analogies

J = *moment of inertia*	m = *mass*
θ = *angular position*	x = *position*
$\dot{\theta}$ = *angular velocity*	$\dot{x}$ = *velocity*
$\ddot{\theta}$ = *angular acceleration*	$\ddot{x}$ = *acceleration*
T = *torque*	F = *force*
$T = J\ddot{\theta}$	$F = m\ddot{x}$

We make a *torque balance*, i.e. a *force balance*. A *torque balance* is usually done at the *drive motor side*, not at, for instance, the *load side*. If so, we have to express all the other relevant *torques* in the system to the *drive motor shaft*, i.e. "*in terms of*" the *drive motor shaft torque*.

Definition 3 A **reflected inertia** is a given inertia (at any point of the system) as seen (through the respective pulleys and/or belts) by the *drive motor shaft*.

Definition 4 **Reflected load inertia** is the *load inertia* as seen by the *drive motor shaft* through pulleys and/or belts.

Definition 5 **Reflected SR pulley assembly inertia** is the *calculated SR pulley assembly inertia* as seen by the *drive motor shaft* through the respective pulleys and/or belts.

Definition 6 Gears that both *drive* and are, in turn, *driven* are called **idler gears**.

The *driving gear* angular displacement and the *driven gear* angular displacement and their derivatives (angular velocity and angular acceleration) are related by the gear ratio n_g in the following manner:

$$r_1\theta_1 = arc = r_2\theta_2$$

$$\frac{\theta_1}{\theta_2} = \frac{r_2}{r_1} = n_g$$

$$\frac{\dot{\theta}_1}{\dot{\theta}_2} = \frac{r_2}{r_1} = n_g$$

$$\frac{\ddot{\theta}_1}{\ddot{\theta}_2} = \frac{r_2}{r_1} = n_g$$

Therefore:

$$\theta_1 = n_g\theta_2 \tag{1}$$

$$\dot{\theta}_1 = n_g \dot{\theta}_2 \tag{2}$$

$$\ddot{\theta}_1 = n_g \ddot{\theta}_2 \tag{3}$$

A *speed reducer* gear train is also a *torque multiplier*.

$$Power = Torque * Angular\ Velocity$$

$$Power_{\ in} = Power_{\ out}$$

$$Torque_{\ in} * Angular\ Velocity_{\ in} = Torque_{\ out} * Angular\ Velocity_{\ out}$$

$$T_{\ in}\, \dot{\theta}_{\ in} = T_{\ out}\, \dot{\theta}_{\ out}$$

$$T_1 \dot{\theta}_1 = T_2 \dot{\theta}_2$$

$$T_2 = \frac{\dot{\theta}_1}{\dot{\theta}_2} T_1 = \frac{r_2}{r_1} T_1$$

Therefore:

$$T_2 = n_g T_1 \tag{4}$$

The torque balance on the load:

$$T_2 = J_2 \ddot{\theta}_2 \tag{5}$$

Substituting (3) and (4), we can rewrite (5) as :

$$n_g T_1 = \frac{J_2}{n_g} \ddot{\theta}_1 \tag{6}$$

rearranging:

$$T_1 = \frac{J_2}{n_g^2} \ddot{\theta}_1 \quad or \quad T_1 = J_{reflected}\, \ddot{\theta}_1 \tag{7}$$

$$J_{reflected} = \frac{J_2}{n_g^2} \tag{8}$$

Equation (7) is the torque equation in "*motor coordinates*".
$J_{reflected}$ is the driven gear inertia (*load inertia*) reflected by the driving gear (*driving motor*) or the load inertia "*felt*" by the driving motor.

This means that the *load inertia* has been reduced by a factor of n_g^2 due to the "*gear train*" from the *motor*'s point of view.

$$\frac{r_2}{r_1} = \frac{N_2}{N_1} = \frac{\theta_1}{\theta_2} = \frac{\dot{\theta}_1}{\dot{\theta}_2} = \frac{\ddot{\theta}_1}{\ddot{\theta}_2} = n_g$$

T is the *torque* on the shaft of the driving gear (motor torque).

The equation of motion for the free body in diagram (a) is:

$$J_1 \ddot{\theta}_1 = T + r_1 F_1 - r_1 F_2 - c_1 \dot{\theta}_1$$

$$J_1 \ddot{\theta}_1 + c_1 \dot{\theta}_1 - r_1 F_1 + r_1 F_2 = T$$

$$J_1 \ddot{\theta}_1 + c_1 \dot{\theta}_1 + r_1 (F_2 - F_1) = T$$

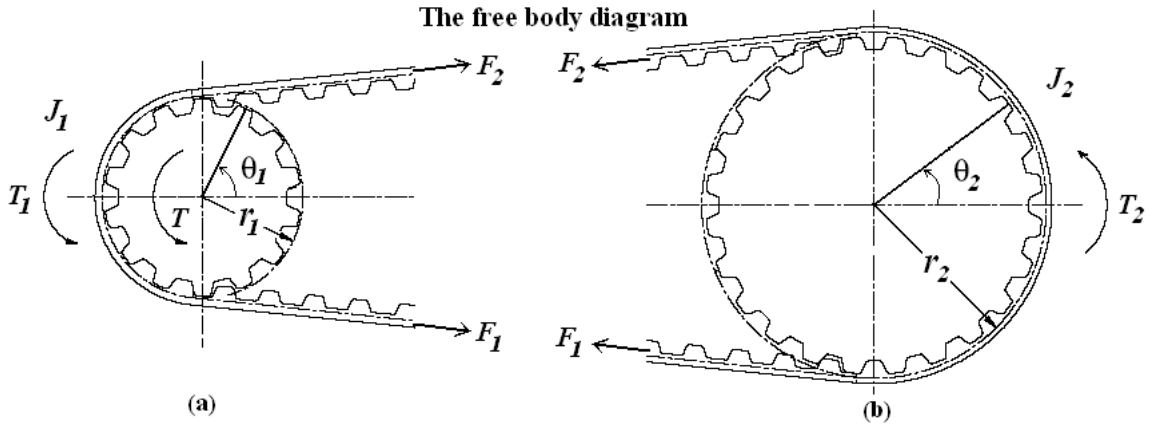

$$F_{belt} = F_2 - F_1$$
$$J_1\ddot{\theta}_1 + c_1\dot{\theta}_1 + r_1\,F_{belt} = T \tag{9}$$

Respectively, the equation of motion for the free body in diagram (b) is:

$$J_2\ddot{\theta}_2 + c_2\dot{\theta}_2 + r_2 F_2 - r_2 F_1 = 0$$

$$J_2\ddot{\theta}_2 + c_2\dot{\theta}_2 - r_2\,(F_1 - F_2) = 0$$

$$J_2\ddot{\theta}_2 + c_2\dot{\theta}_2 - r_2 F_{belt} = 0 \tag{10}$$

$$\frac{r_2}{r_1} = \frac{\theta_1}{\theta_2} = \frac{\dot{\theta}_1}{\dot{\theta}_2} = \frac{\ddot{\theta}_1}{\ddot{\theta}_2} \tag{11}$$

$$F_{belt} = \frac{J_2}{r_2}\ddot{\theta}_2 + \frac{c_2}{r_2}\dot{\theta}_2 \tag{12}$$

The *three relevant* equations are:

$$\begin{cases} J_1\ddot{\theta}_1 + c_1\dot{\theta}_1 + r_1\,F_{belt} = T \\ J_2\ddot{\theta}_2 + c_2\dot{\theta}_2 - r_2\,F_{belt} = 0 \\ \dfrac{r_2}{r_1} = \dfrac{\theta_1}{\theta_2} = \dfrac{\dot{\theta}_1}{\dot{\theta}_2} = \dfrac{\ddot{\theta}_1}{\ddot{\theta}_2} = n_g \end{cases}$$

Substituting (14) in (12)

$$J_1\left(\frac{r_2}{r_1}\right)\ddot{\theta}_2 + c_1\left(\frac{r_2}{r_1}\right)\dot{\theta}_2 + F_{belt}\,r_1 = T \tag{13}$$

Substituting (15) in (16), and then multiplying by $\dfrac{r_2}{r_1}$

$$J_1\left(\frac{r_2}{r_1}\right)\ddot{\theta}_2 + c_1\left(\frac{r_2}{r_1}\right)\dot{\theta}_2 + J_2\left(\frac{r_1}{r_2}\right)\ddot{\theta}_2 + c_2\left(\frac{r_1}{r_2}\right)\dot{\theta}_2 = T \quad \Big| * \frac{r_2}{r_1} \tag{14}$$

It results:

$$\left[J_1\left(\frac{r_2}{r_1}\right)^2 + J_2\right]\ddot{\theta}_2 + \left[c_1\left(\frac{r_2}{r_1}\right)^2 + c_2\right]\dot{\theta}_2 = \frac{r_2}{r_1}\,T \tag{15}$$

or

$$\left[J_1 n_g^2 + J_2\right]\ddot{\theta}_2 + \left[c_1 n_g^2 + c_2\right]\dot{\theta}_2 = n_g T \tag{16}$$

2.1.2 Three-gear belt mechanism - M220 Industrial Emulator

The M220 diagram shows a three-gear belt mechanism and is presented in the figure below:

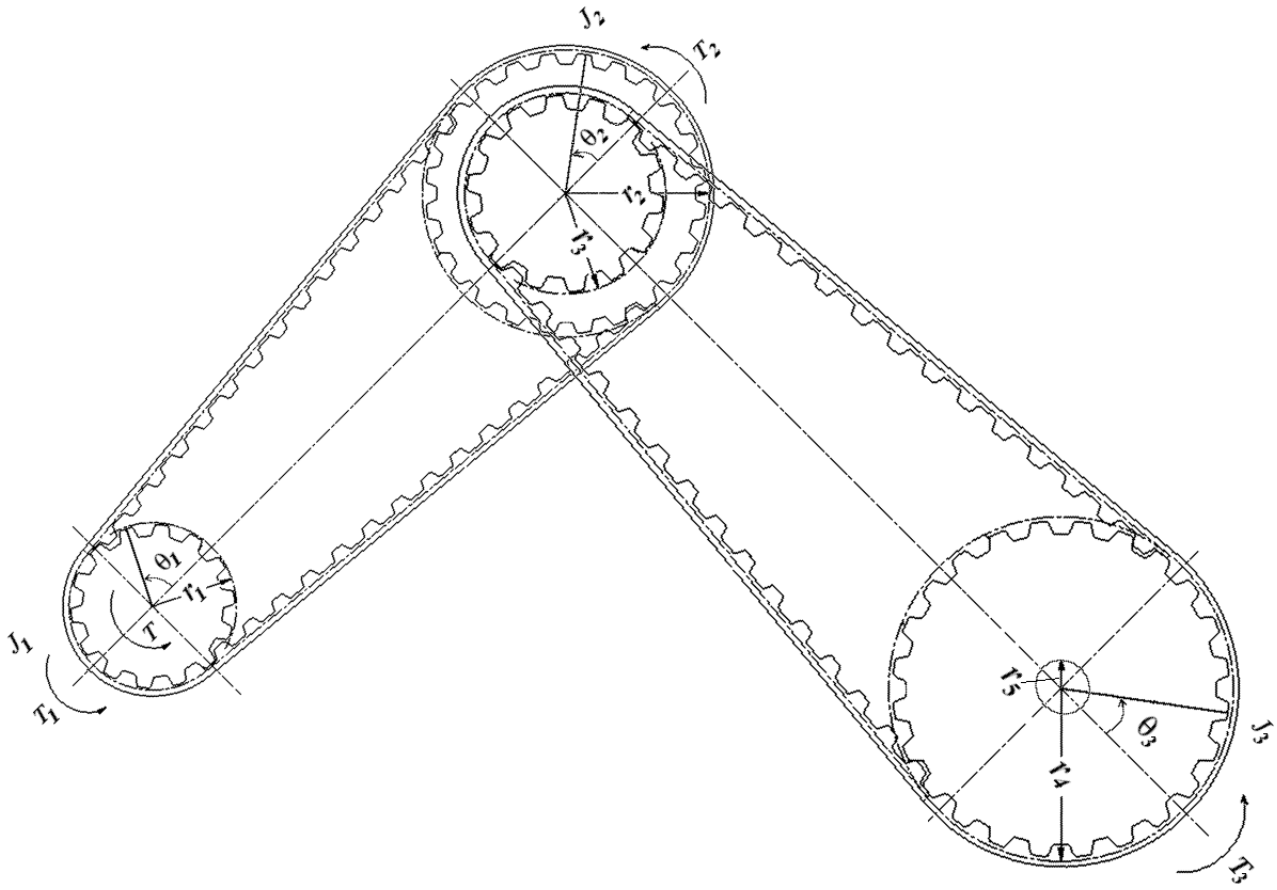

It can be observed that the system can be decomposed into three parts, see *body-free diagram* for more details. T is the *torque* on the shaft of the driving gear (motor torque).

Firstly, the *equation of motion* for the free body in diagram (a) is:

$$J_1\ddot{\theta}_1 = T + r_1\,F_1 - r_1\,F_2 - c_1\dot{\theta}_1$$

$$J_1\ddot{\theta}_1 + c_1\dot{\theta}_1 - r_1\,F_1 + r_1\,F_2 = T$$

$$J_1\ddot{\theta}_1 + c_1\dot{\theta}_1 + r_1\,(F_2 - F_1) = T$$

$$F_{belt_1} = F_2 - F_1$$

$$J_1\ddot{\theta}_1 + c_1\dot{\theta}_1 + r_1\,F_{belt_1} = T \tag{17}$$

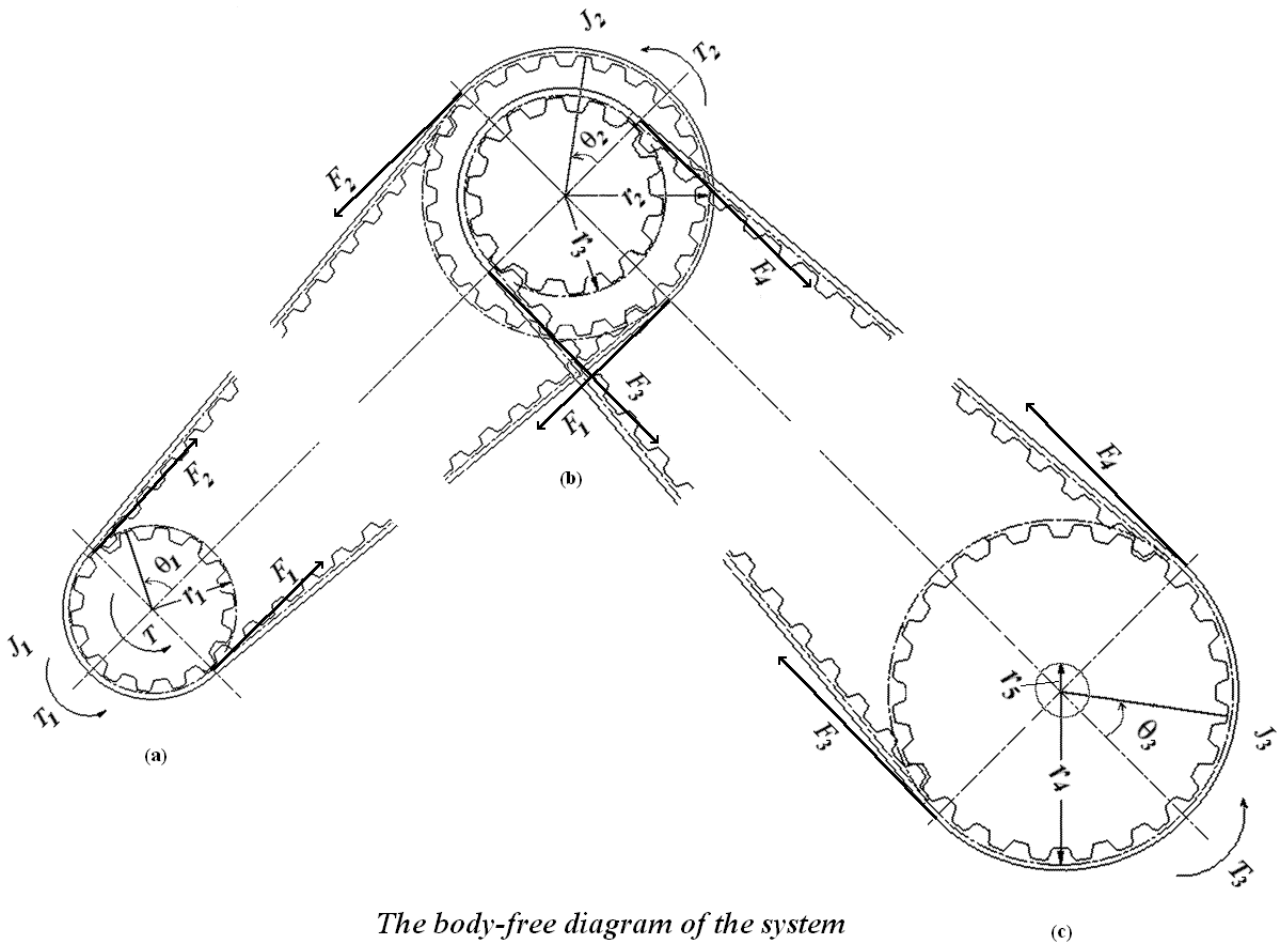

The body-free diagram of the system

Secondly, the *equation of motion* for the free body in diagram (b) is:

$$J_2\ddot{\theta}_2 = 0 - r_2F_1 + r_2F_2 + r_3F_3 - r_3F_4 - c_2\dot{\theta}_2$$

$$J_2\ddot{\theta}_2 + c_2\dot{\theta}_2 + r_2F_1 - r_2F_2 - r_3F_3 + r_3F_4 = 0$$

$$J_2\ddot{\theta}_2 + c_2\dot{\theta}_2 - r_2(F_2 - F_1) + r_3(F_4 - F_3) = 0$$

$$F_{belt_1} = F_2 - F_1 \quad F_{belt_2} = F_4 - F_3$$

$$J_2\ddot{\theta}_2 + c_2\dot{\theta}_2 - r_2F_{belt_1} + r_3F_{belt_2} = 0$$

$$\frac{r_2}{r_1} = \frac{\theta_1}{\theta_2} = \frac{\dot{\theta}_1}{\dot{\theta}_2} = \frac{\ddot{\theta}_1}{\ddot{\theta}_2} = \frac{n_{pd}}{n} = n'_g$$

Thirdly, the *equation of motion* for the free body in diagram (c) is:

$$J_3\ddot{\theta}_3 = 0 + r_4F_4 - r_4F_3 - c_3\dot{\theta}_3 - r_5\,F_c\,\mathrm{sgn}(\dot{\theta}_3)$$

$$J_3\ddot{\theta}_3 + c_3\dot{\theta}_3 - r_4F_4 + r_4F_3 + r_5\,F_c\,\mathrm{sgn}(\dot{\theta}_3) = 0$$

$$J_3\ddot{\theta}_3 + c_3\dot{\theta}_3 - r_4(F_4 - F_3) + r_5\,F_c\,\mathrm{sgn}(\dot{\theta}_3) = 0$$

$$J_3\ddot{\theta}_3 + c_3\dot{\theta}_3 - r_4 F_{belt_2} + r_5\, F_c \operatorname{sgn}(\dot{\theta}_3) = 0 \tag{18}$$

$$\frac{r_4}{r_3} = \frac{\theta_2}{\theta_3} = \frac{\dot{\theta}_2}{\dot{\theta}_3} = \frac{\ddot{\theta}_2}{\ddot{\theta}_3} = \frac{N}{n_{pl}} = n_g'' \tag{19}$$

The *five relevant* equations are:

$$\begin{cases} J_1\ddot{\theta}_1 + c_1\dot{\theta}_1 + r_1\, F_{belt_1} = T \\ J_2\ddot{\theta}_2 + c_2\dot{\theta}_2 - r_2\, F_{belt_1} + r_3\, F_{belt_2} = 0 \\ \dfrac{r_2}{r_1} = \dfrac{\theta_1}{\theta_2} = \dfrac{\dot{\theta}_1}{\dot{\theta}_2} = \dfrac{\ddot{\theta}_1}{\ddot{\theta}_2} = \dfrac{n_{pd}}{n} = n_g' \\ J_3\ddot{\theta}_3 + c_3\dot{\theta}_3 - r_4 F_{belt_2} + r_5\, F_c \operatorname{sgn}(\dot{\theta}_3) = 0 \\ \dfrac{r_4}{r_3} = \dfrac{\theta_2}{\theta_3} = \dfrac{\dot{\theta}_2}{\dot{\theta}_3} = \dfrac{\ddot{\theta}_2}{\ddot{\theta}_3} = \dfrac{N}{n_{pl}} = n_g'' \end{cases}$$

And it results:

$$F_{belt_2} = \frac{J_3}{r_4}\ddot{\theta}_3 + \frac{c_3}{r_4}\dot{\theta}_3 + \frac{r_5}{r_4}\, F_c \operatorname{sgn}(\dot{\theta}_3)$$

$$F_{belt_1} = -\frac{1}{r_2}\Big[- r_3\, F_{belt_2} - J_2\ddot{\theta}_2 - c_2\dot{\theta}_2\Big] = \frac{1}{r_2}\Big[r_3\, F_{belt_2} + J_2\ddot{\theta}_2 + c_2\dot{\theta}_2\Big]$$

$$J_1\ddot{\theta}_1 + c_1\dot{\theta}_1 + r_1\, \frac{1}{r_2}\Big[r_3\, F_{belt_2} + J_2\ddot{\theta}_2 + c_2\dot{\theta}_2\Big] = T$$

$$J_1\ddot{\theta}_1 + c_1\dot{\theta}_1 + r_1\, \frac{1}{r_2}\Big[r_3\, \Big(\frac{J_3}{r_4}\ddot{\theta}_3 + \frac{c_3}{r_4}\dot{\theta}_3 + \frac{r_5}{r_4}\, F_c \operatorname{sgn}(\dot{\theta}_3)\Big) + J_2\ddot{\theta}_2 + c_2\dot{\theta}_2\Big] = T$$

$$\frac{r_2}{r_1} = \frac{\theta_1}{\theta_2}$$

$$\frac{r_4}{r_3} = \frac{\theta_2}{\theta_3}$$

$$\theta_2 = \frac{r_4\theta_3}{r_3}$$

$$\frac{r_2}{r_1} = \frac{\theta_1}{\frac{r_4\theta_3}{r_3}}$$

$$\theta_1 = \frac{r_2 r_4\theta_3}{r_1 r_3} = n_g' n_g''\theta_3 = n_g\theta_3$$

$$\theta_2 = \frac{r_4\theta_3}{r_3}$$

$$J_1\frac{r_2 r_4\ddot{\theta}_3}{r_1 r_3} + c_1\frac{r_2 r_4\dot{\theta}_3}{r_1 r_3}{}_1 + r_1\, \frac{1}{r_2}\Big[r_3\, \Big(\frac{J_3}{r_4}\ddot{\theta}_3 + \frac{c_3}{r_4}\dot{\theta}_3 + \frac{r_5}{r_4}\, F_c \operatorname{sgn}(\dot{\theta}_3)\Big) + J_2\frac{r_4\ddot{\theta}_3}{r_3} + c_2\frac{r_4\dot{\theta}_3}{r_3}\Big] = T$$

$$\Big[J_1\frac{r_2 r_4}{r_1 r_3} + J_3\frac{r_1 r_3}{r_2 r_4} + J_2\frac{r_1 r_4}{r_2 r_3}\Big]\ddot{\theta}_3 + \Big[c_1\frac{r_2 r_4}{r_1 r_3} + c_3\frac{r_1 r_3}{r_2 r_4} + c_2\frac{r_1 r_4}{r_2 r_3}\Big]\dot{\theta}_3 + \frac{r_1 r_3}{r_2 r_4}\, r_5\, F_c \operatorname{sgn}(\dot{\theta}_3) = T$$

Then multiplying by $\dfrac{r_2}{r_1}\dfrac{r_4}{r_3}$

$$\Big[J_1\Big(\frac{r_2 r_4}{r_1 r_3}\Big)^2 + J_3 + J_2\Big(\frac{r_4}{r_3}\Big)^2\Big]\ddot{\theta}_3 + \Big[c_1\Big(\frac{r_2 r_4}{r_1 r_3}\Big)^2 + c_3 + c_2\Big(\frac{r_4}{r_3}\Big)^2\Big]\dot{\theta}_3 + r_5\, F_c \operatorname{sgn}(\dot{\theta}_3) = \frac{r_2}{r_1}\frac{r_4}{r_3}T$$

$$\Big[J_1 n_g^2 + J_2 n_g''^2 + J_3\Big]\ddot{\theta}_3 + \Big[c_1 n_g^2 + c_2 n_g''^2 + c_3\Big]\dot{\theta}_3 + r_5\, F_c \operatorname{sgn}(\dot{\theta}_3) = n_g T$$

$$J_{total}\,\ddot{\theta} + c\,\dot{\theta} + f\,\mathrm{sgn}(\dot{\theta}) = n_g T$$

where:

$$J_{total} = J_1 n_g^2 + J_2 n_g''^2 + J_3$$

$$c = c_1 n_g^2 + c_2 n_g''^2 + c_3$$

$$f = r_5\, F_c$$

$$\theta = \theta_3$$

T is the *torque* on the shaft of the driving gear (motor torque).
n is the number of teeth on the drive disk pulley, **fixed number**; $n = 12$.
N is the number of teeth on the load disk pulley, **fixed number**; $N = 72$.
n_{pd} is the number of teeth on the bottom pulley.
n_{pl} is the number of teeth on the top pulley.
n_g is the *total gear ratio*.

$$\text{where} \quad n_g = \frac{N}{n_{pl}}\frac{n_{pd}}{n} = \frac{72}{n_{pl}}\frac{n_{pd}}{12} = \frac{6\,n_{pd}}{n_{pl}}$$

n_g' is the *partial first gear ratio*.

$$\text{where} \quad n_g' = \frac{n_{pd}}{n} = \frac{n_{pd}}{12}$$

n_g'' is the *partial second gear ratio*.

$$\text{where} \quad n_g'' = \frac{N}{n_{pl}} = \frac{72}{n_{pl}}$$

If we write:

$$J_{total} = J_1 n_g^2 + J_2 n_g''^2 + J_3$$

as

$$\frac{J_{total}}{n_g^2} = J_1 + J_2\frac{n_g''^2}{n_g^2} + \frac{J_3}{n_g^2}$$

$$J = \frac{J_{total}}{n_g^2} = J_1 + \frac{J_2}{n_g'^2} + \frac{J_3}{n_g^2}$$

Now, if we look at the *reflected inertia* in the equation (10):

$$J_d = J_{dd} + J_{wd} + \frac{J_p}{(n_g')^2} + \frac{J_{dl} + J_{wl}}{(n_g)^2}$$

We can identify the following:

$$J_d = \frac{J_{total}}{n_g^2} = J$$

$$J_1 = J_{dd} + J_{wd}$$

$$J_2 = J_p$$

$$J_3 = J_{dl} + J_{wl}$$

From the M220 manual [28]:

$J_{dd} = 0.00040$ kg-m^2
$J_{drive\ disk} = 0.000381$ kg-m^2
$J_{motor} = 3.8 * 10^{-5}$ kg-m^2 - (from manufacturer specifications)
Diameter of the *drive disk* is: 13.21 cm.
Thickness of the *drive disk plate* = 0.47 cm. $\rho_{aluminum} = 2.71$g/cm^3

A *brass weight* has 500 g (including *attachment bolts* and *nuts*).
The *inertia* of the *cutout slots* on the drive load and disks is negligible.
The inertia of the encoder, and the belt and pulleys between the motor and the drive disk can be neglected too.
The *calculated mass* of drive disk is 0.174 kg.

System Dynamic Parameters

Parameter	Value
J_{dd}	0.00040 kg-m^2
J_{dl}	0.0065 kg-m^2
$J_{dl} - J_{d.c.motor}$	0.0065 kg-m^2 – 0.000038 kg-m^2
J_{wd} (with 4 *0.20 kg masses at r = 5.0 cm)†	0.0021 kg-m^2
J_{wl} (with 4 *0.50 kg masses at r = 10.0 cm)†	0.0206 kg-m^2
c_1 (drive friction (modeled as viscous)). No belt to SR assembly	0.002 N-m/rad/s (approximately)
c_1 (drive friction (modeled as viscous)). Belt connected to SR assembly	0.004 N-m/rad/s (approximately)
c_2 (load friction at load (modeled as viscous)) Includes load disk-to-SR belt	0.05 N-m/rad/s (approximately)

† Includes inertia of weights about their c.g. (center of gravity)

SR Pulley Inertia Values

Number of Pulley Teeth	Pulley Inertia, J_p (kg-m^2)
18 tooth	3 * 10^{-6}
24 tooth	8 * 10^{-6}
36 tooth	3.9 * 10^{-5}
72 tooth	5.5 * 10^{-4}
Backlash device (incl. attachment screws) – add to J_p	3.1 * 10^{-5}

2.1.3 The Inertia Balance

$$J_d = (J_{dd} + J_{dl} + J_{wd} + J_{wl} + J_p)_{reflected} \tag{20}$$

where

J_{dd} is the inertia of the bare drive disk plus the drive motor, encoder, drive disk/motor belt, and pulleys.
J_{dl} is the inertia of the bare load disk plus the disturbance motor, encoder, load disk/motor belt, and pulleys.
J_{wd} is the inertia associated with the brass weights at the drive disk.
J_{wl} is the inertia associated with the brass weights at the load disk.
J_p is the inertia associated with the pulleys in the SR assembly.

$$J_{dd} = J_{bare\ drive\ disk} + J_{drive\ motor} + J_{encoder\ 1} + J_{drive\ disk/motor\ belt} + J_{drive\ disk\ pulley} + J_{drive\ motor\ pulley}$$

$$J_{dl} = J_{bare\ load\ disk} + J_{\textbf{disturbance motor}} + J_{encoder\ 2} + J_{load\ disk/motor\ belt} + J_{load\ disk\ pulley} + J_{load\ motor\ pulley}$$

$$\begin{aligned} J_d = (&J_{bare\ drive\ disk} + J_{drive\ motor} + J_{encoder\ 1} + J_{drive\ disk/motor\ belt} + J_{drive\ disk\ pulley} + J_{drive\ motor\ pulley} + \\ &+ J_{bare\ load\ disk} + J_{\textbf{disturbance motor}} + J_{encoder\ 2} + J_{load\ disk/motor\ belt} + J_{load\ disk\ pulley} + \\ &+ J_{load\ motor\ pulley} + J_{drive\ disk\ brass\ weights} + J_{load\ disk\ brass\ weights} + J_{SR\ assembly\ pulleys} + \\ &+ J_{top\ pulley\ belt} + J_{bottom\ pulley\ belt})_{reflected\ to\ the\ drive\ motor\ shaft} \end{aligned}$$

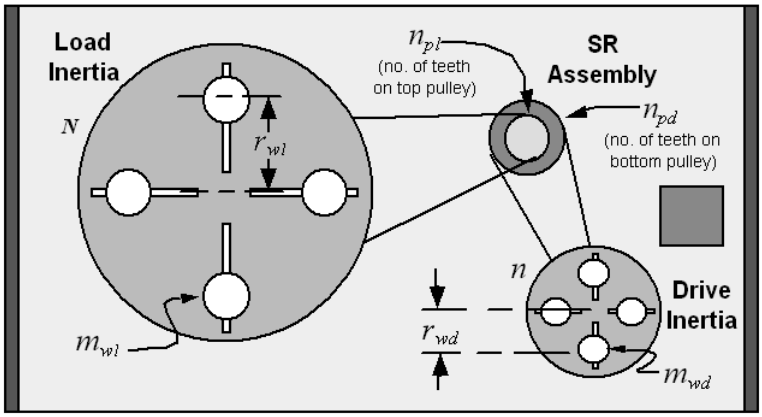

Because the **reflected inertia** of a given component is *inversely proportional* to the *square of its the gear ratio* to the motor shaft - see equation (8) - we have:

$$J_d = J_{dd} + J_{wd} + \frac{J_p}{(n'_g)^2} + \frac{J_{dl} + J_{wl}}{(n_g)^2}. \tag{21}$$

where

n is the number of teeth on the drive disk pulley, **fixed number**; $n = 12$.
N is the number of teeth on the load disk pulley, **fixed number**; $N = 72$.
n_{pd} is the number of teeth on the bottom pulley.
n_{pl} is the number of teeth on the top pulley.
n_g is the *total gear ratio* (between the **Drive Inertia** and the **Load Inertia**).

where $n_g = \frac{N}{n_{pl}} \frac{n_{pd}}{n} = \frac{72}{n_{pl}} \frac{n_{pd}}{12} = \frac{6 n_{pd}}{n_{pl}}$

n'_g is the *partial gear ratio* (between the **Drive Inertia** and **SR Assembly**).

where $n'_g = \frac{n_{pd}}{n} = \frac{n_{pd}}{12}$

r_{wd} is the distance between the center of the drive disk and brass weights on it, in *centimeters*.
r_{wl} is the distance between the center of the load disk and brass weights on it

in *centimeters*.
m_{wd} is the total mass of the brass weights on the drive disk, in *kilograms*.
m_{wl} is the total mass of the brass weights on the load disk, in *kilograms*.

Thus, we can rewrite equation (10) as:

$$J_d = J_{dd} + J_{wd} + \frac{J_p}{\left(\frac{n_{pd}}{12}\right)^2} + \frac{J_{dl} + J_{wl}}{\left(\frac{6n_{pd}}{n_{pl}}\right)^2} \tag{22}$$

The primary types of **resistance** in M220 are:

Elastic resistance - resistance proportional to *displacement*.
Static friction - initial resistance to *the beginning of motion*.
Coulomb friction - resistance to *motion*.
Viscous damping - resistance proportional to *velocity*.
Inertia - resistance proportional to *acceleration*.

2.1.4 Plant continuous and discrete transfer functions

Let us ignore the friction force for a moment and calculate the continuous and discrete plant transfer functions.

Continuous time transfer function

$$J\ddot{\theta} + c\dot{\theta} = n_g T$$

$$J\,\frac{d^2\theta(t)}{dt^2} + c\,\frac{d\theta(t)}{dt} = n_g T(t)$$

$$\mathcal{L}\left\{\frac{d\theta(t)}{dt}\right\} = s\,\theta(s) - \theta(0)$$

$$\mathcal{L}\left\{\frac{d^2\theta(t)}{dt^2}\right\} = s^2\,\theta(s) - s\,\theta(0) - \dot{\theta}(0)$$

$$\mathcal{L}\{T(t)\} = T(s)$$

Using *zero initial conditions* we can rewrite:

$$J s^2\,\theta(s) + c\,s\,\theta(s) = n_g T(s)$$

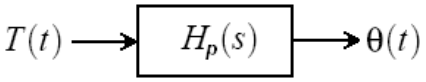

Then the plant's continuous transfer function is:

$$H(s) = \frac{\theta(s)}{T(s)} = \frac{n_g}{J s^2 + c\,s}$$

There are no zeros and two poles at:

$$p_{s1} = 0$$
$$p_{s2} = -\frac{c}{J}$$

The gain is

$$k = \frac{n_g}{J}$$

So

$$H(s) = \frac{k}{(s - p_{s1})(s - p_{s2})} \qquad \text{or} \qquad H(s) = \frac{k}{s(s - p_{s2})}$$

Discrete time transfer function

Zero-order hold for our continuous plant gives:

$$H(z) = (1-z^{-1})\mathcal{Z}\left[\mathcal{L}^{-1}\left\{\frac{H(s)}{s}\right\}\right] = (1-z^{-1})\mathcal{Z}\left[\mathcal{L}^{-1}\left\{\frac{\frac{n_g}{Js^2+cs}}{s}\right\}\right]$$

$$\mathcal{L}^{-1}\left\{\frac{\frac{n_g}{Js^2+cs}}{s}\right\} = \mathcal{L}^{-1}\left\{\frac{n_g}{s(Js^2+cs)}\right\}$$

$$\frac{n_g}{s(Js^2+cs)} = \frac{P}{s^2}+\frac{Q}{s}+\frac{R}{Js+c} = \frac{P(Js+c)}{s^2}+\frac{Qs(Js+c)}{s}+\frac{Rs^2}{Js+c}$$

$$P(Js+c)+Qs(Js+c)+Rs^2 = n_g$$

$$(R+QJ)s^2+(PJ+QJ)s+Pc = n_g$$

$$\begin{cases} Pc & = & n_g \\ R+QJ & = & 0 \\ PJ+Qc & = & 0 \end{cases}$$

$$P = \frac{n_g}{c}$$

$$Q = \frac{-PJ}{c} = \frac{-R}{J}$$

Thus

$$P = \frac{n_g}{c} \quad Q = \frac{-n_g J}{c^2} \quad R = \frac{n_g J^2}{c^2}$$

So we have

$$\mathcal{L}^{-1}\left\{\frac{n_g}{s(Js^2+cs)}\right\} = \mathcal{L}^{-1}\left\{\frac{P}{s^2}+\frac{Q}{s}+\frac{R}{Js+c}\right\} = \mathcal{L}^{-1}\left\{\frac{P}{s^2}+\frac{Q}{s}+\frac{\frac{R}{J}}{s+\frac{c}{J}}\right\} = Pt+Q+\frac{R}{J}e^{-\frac{c}{J}t}$$

$$\mathcal{L}^{-1}\left\{\frac{n_g}{s(Js^2+cs)}\right\} = Pt+Q+\frac{R}{J}e^{-\frac{c}{J}t} = \frac{n_g}{c}t+\frac{-n_g J}{c^2}+\frac{n_g J}{c^2}e^{-\frac{c}{J}t} = \frac{n_g}{c}t-\frac{n_g J}{c^2}+\frac{n_g J}{c^2}e^{-\frac{c}{J}t}$$

$$H(z) = (1-z^{-1})\mathcal{Z}\left[\mathcal{L}^{-1}\left\{\frac{H(s)}{s}\right\}\right] = (1-z^{-1})\mathcal{Z}\left[\frac{n_g}{c}t-\frac{n_g J}{c^2}+\frac{n_g J}{c^2}e^{-\frac{c}{J}t}\right] = (1-z^{-1})\frac{n_g}{c^2}\mathcal{Z}\left[ct-J+Je^{-\frac{c}{J}t}\right]$$

$$H(z) = \frac{n_g}{c^2}\frac{z-1}{z}\left[c\frac{T_s z}{(z-1)^2}-J\frac{z}{(z-1)}+J\frac{z}{z-e^{-\frac{c}{J}T_s}}\right] = \frac{n_g}{c^2}\left[\frac{cT_s}{(z-1)}-J+J\frac{z-1}{z-e^{-\frac{c}{J}T_s}}\right]$$

$$H(z) = \frac{n_g}{c^2}\frac{cT_s(z-e^{-\frac{c}{J}T_s})-J(z-1)(z-e^{-\frac{c}{J}T_s})+J(z-1)^2}{(z-1)(z-e^{-\frac{c}{J}T_s})} = \frac{n_g}{c^2}\frac{cT_s[z-e^{-\frac{c}{J}T_s}]-J[z^2-ze^{-\frac{c}{J}T_s}-z+e^{-\frac{c}{J}T_s}]+J[z^2-2z+1]}{z^2-ze^{-\frac{c}{J}T_s}-z+e^{-\frac{c}{J}T_s}}$$

$$H(z) = \frac{n_g}{c^2}\frac{cT_s z-cT_s e^{-\frac{c}{J}T_s}\cancel{-Jz^2}+Jze^{-\frac{c}{J}T_s}+Jz-Je^{-\frac{c}{J}T_s}\cancel{+Jz^2}-2Jz+J}{z^2-z[e^{-\frac{c}{J}T_s}+1]+e^{-\frac{c}{J}T_s}} = \frac{n_g}{c^2}\frac{z[cT_s+Je^{-\frac{c}{J}T_s}-J]-cT_s e^{-\frac{c}{J}T_s}-Je^{-\frac{c}{J}T_s}+J}{z^2-z[e^{-\frac{c}{J}T_s}+1]+e^{-\frac{c}{J}T_s}} = \frac{order\ 1}{order\ 2}$$

$$H(z) = \frac{\beta_1 z+\beta_2}{z^2+\alpha_1 z+\alpha_2} = \frac{order\ 1}{order\ 2}$$

where:

$$\alpha_1 = -[e^{-\frac{c}{J}T_s}+1]$$

Laplace Domain	Time domain	Z Domain ($t=nT_s$)
1	$\delta(t)$ unit impulse	1
$\frac{1}{s}$	$u(t)$ unit step	$\frac{z}{z-1}$
$\frac{1}{s^2}$	t	$\frac{T_s z}{(z-1)^2}$
$\frac{1}{s+a}$	e^{-at}	$\frac{z}{z-e^{-aT_s}}$
$\frac{b}{(s+a)^2+b^2}$	$e^{-at}\sin(bt)$	$\frac{ze^{-aT_s}\sin(bT_s)}{z^2-2ze^{-aT_s}\cos(bT_s)+e^{-2aT_s}}$
$\frac{s+a}{(s+a)^2+b^2}$	$e^{-at}\cos(bt)$	$\frac{z^2-ze^{-aT_s}\cos(bT_s)}{z^2-2ze^{-aT_s}\cos(bT_s)+e^{-2aT_s}}$
$\frac{As+B}{s^2+2as+c}$	$e^{-at}\left[A\cos(bt)+\frac{B-aA}{b}\sin(bt)\right]$ $b=\sqrt{c-a^2}$	

$$\alpha_2 = e^{-\frac{c}{J}T_s}$$

$$\beta_1 = \frac{n_g}{c^2}[cT_s + Je^{-\frac{c}{J}T_s} - J]$$

$$\beta_2 = \frac{n_g}{c^2}[-cT_s e^{-\frac{c}{J}T_s} - Je^{-\frac{c}{J}T_s} + J]$$

Furthermore

$$H(z) = \frac{\beta_1 z + \beta_2}{z^2 + \alpha_1 z + \alpha_2} = \frac{z(\beta_1 + \beta_2 \frac{1}{z})}{z^2(1 + \alpha_1 \frac{1}{z} + \alpha_2 \frac{1}{z^2})} = \frac{1}{z}\frac{(\beta_1 + \beta_2 \frac{1}{z})}{(1 + \alpha_1 \frac{1}{z} + \alpha_2 \frac{1}{z^2})}$$

or

$$H(z^{-1}) = z^{-1}\frac{(\beta_1 + \beta_2 z^{-1})}{(1 + \alpha_1 z^{-1} + \alpha_2 z^{-2})} = \frac{\beta_1 z^{-1} + \beta_2 z^{-2}}{1 + \alpha_1 z^{-1} + \alpha_2 z^{-2}}$$

or using the *backward shift operator:*

$$H(q^{-1}) = \frac{\beta_1 q^{-1} + \beta_2 q^{-2}}{1 + \alpha_1 q^{-1} + \alpha_2 q^{-2}} = \frac{B(q^{-1})}{A(q^{-1})}$$

There is one zero:

$$z_{z1} = -\frac{\beta_2}{\beta_1} \qquad \text{Note that the gain is} \quad k = \beta_1 = \frac{n_g}{c^2}[cT_s + Je^{-\frac{c}{J}T_s} - J]$$

$$z_{z1} = -\frac{\frac{n_g}{c^2}[-cT_s e^{-\frac{c}{J}T_s} - Je^{-\frac{c}{J}T_s} + J]}{\frac{n_g}{c^2}[cT_s + Je^{-\frac{c}{J}T_s} - J]} = \frac{cT_s e^{-\frac{c}{J}T_s} + Je^{-\frac{c}{J}T_s} - J}{cT_s + Je^{-\frac{c}{J}T_s} - J} = \frac{cT_s e^{-\frac{c}{J}T_s} - cT_s + cT_s + Je^{-\frac{c}{J}T_s} - J}{cT_s + Je^{-\frac{c}{J}T_s} - J} =$$

$$z_{z1} = \frac{c\,T_s e^{-\frac{c}{J}T_s} - c\,T_s}{c\,T_s + Je^{-\frac{c}{J}T_s} - J} + 1 = \frac{c\,T_s\left[e^{-\frac{c}{J}T_s} - 1\right]}{c\,T_s + J\left[e^{-\frac{c}{J}T_s} - 1\right]} + 1 = \frac{\left[e^{-\frac{c}{J}T_s} - 1\right]}{1 + \frac{\left[e^{-\frac{c}{J}T_s} - 1\right]}{\frac{c}{J}T_s}} + 1 = 1 - \frac{\left[1 - e^{-\frac{c}{J}T_s}\right]}{1 - \frac{\left[1 - e^{-\frac{c}{J}T_s}\right]}{\frac{c}{J}T_s}}$$

$$\left\{\frac{c}{J}T_s = x\right\} \qquad z_{z1} = 1 - \frac{\left[1 - e^{-x}\right]}{1 - \frac{\left[1 - e^{-x}\right]}{x}} \simeq 1 - \frac{\left[1 - 1 + \frac{x}{1!} - \frac{x^2}{2!}\right]}{1 - \frac{\left[1 - 1 + \frac{x}{1!} - \frac{x^2}{2!}\right]}{x}} \simeq 1 - \frac{\left[\frac{x}{1!} - \frac{x^2}{2!}\right]}{\frac{x}{2}}$$

$$\left\{e^{ax} = 1 + \frac{ax}{1!} + \frac{a^2x^2}{2!} + \frac{a^3x^3}{3!} + \ldots\right\} \qquad z_{z1} \simeq 1 - \frac{\cancel{x}\left[1 - \frac{x}{2}\right]}{\cancel{\frac{x}{2}}} \simeq 1 - 2\left[1 - \frac{x}{2}\right] \simeq -1 + x \simeq -1 + \frac{c}{J}T_s$$

And two poles:

$$p_{z1} = \frac{-\alpha_1 + \sqrt{\alpha_1^2 - 4\alpha_2}}{2} \qquad p_{z2} = \frac{-\alpha_1 - \sqrt{\alpha_1^2 - 4\alpha_2}}{2}$$

$$\sqrt{\alpha_1^2 - 4\alpha_2} = \sqrt{-[e^{-\frac{c}{J}T_s} + 1]^2 - 4e^{-\frac{c}{J}T_s}} = \sqrt{e^{-\frac{2c}{J}T_s} + 2e^{-\frac{c}{J}T_s} + 1 - 4e^{-\frac{c}{J}T_s}} = \sqrt{e^{-\frac{2c}{J}T_s} - 2e^{-\frac{c}{J}T_s} + 1} =$$

$$= \sqrt{(1 - e^{-\frac{c}{J}T_s})^2} = 1 - e^{-\frac{c}{J}T_s}$$

$$p_{z1} = \frac{\cancel{e^{-\frac{c}{J}T_s}} + 1 + 1 \cancel{- e^{-\frac{c}{J}T_s}}}{2} = \frac{2}{2} = 1$$

$$p_{z2} = \frac{e^{-\frac{c}{J}T_s} + \cancel{1} - \cancel{1} + e^{-\frac{c}{J}T_s}}{2} = \frac{2e^{-\frac{c}{J}T_s}}{2} = e^{-\frac{c}{J}T_s}$$

So

$$H(z) = \frac{k\,(z - z_{z1})}{(z - p_{z1})(z - p_{z2})}$$

where

$$k = \frac{n_g}{c^2}[c\,T_s + Je^{-\frac{c}{J}T_s} - J]$$

$$z_{z1} = -1 + \frac{c}{J}T_s$$

$$p_{z1} = 1$$

$$p_{z2} = e^{-\frac{c}{J}T_s}$$

Observation 1: $\frac{J}{c} > 1$.

Observation 2: The **two poles** can be written in two equivalent ways and also the **zero**.

The **poles** can be written as:

$$p_{z_1} = 1 \qquad p_{z_2} = e^{-\frac{cT_s}{J}}$$

$$p_{z_1} = \frac{-\alpha_1 - \sqrt{\alpha_1^2 - 4\alpha_2}}{2} \qquad p_{z_2} = \frac{-\alpha_1 + \sqrt{\alpha_1^2 - 4\alpha_2}}{2}$$

$$p_{z_1} = \frac{-\alpha_1 + \sqrt{\alpha_1^2 - 4\alpha_2}}{2} = \frac{e^{-\lambda} + 1 - \sqrt{(-[e^{-\lambda}+1])^2 - 4e^{-\lambda}}}{2} = \frac{e^{-\lambda} + 1 - \sqrt{e^{-2\lambda} + 2e^{-\lambda} - 4e^{-\lambda} + 1}}{2}$$

$$p_{z_1} = \frac{(e^{-\lambda}+1) - \sqrt{(e^{-\lambda}-1)^2}}{2} = \frac{\cancel{e^{-\lambda}} + 1 \cancel{- e^{-\lambda}} + 1}{2} = 1$$

$$p_{z_2} = \frac{(e^{-\lambda}+1) + \sqrt{(e^{-\lambda}-1)^2}}{2} = \frac{e^{-\lambda} \cancel{+1} + e^{-\lambda} \cancel{-1}}{2} = e^{-\lambda} \qquad \text{where} \quad \lambda = -\frac{cT_s}{J}$$

And the **zero** as:

$$z_{z_1} = -\frac{\beta_1}{\beta_2} = -\frac{\frac{n\cancel{q}}{\cancel{c^2}}\left[c\,T_s + Je^{-\frac{c}{J}T_s} - J\right]}{\frac{n\cancel{q}}{\cancel{c^2}}\left[-c\,T_s e^{-\frac{c}{J}T_s} - Je^{-\frac{c}{J}T_s} + J\right]} = \frac{\cancel{J}\left[\frac{c\,T_s}{J} + e^{-\frac{c}{J}T_s} - 1\right]}{\cancel{J}\left[\frac{c\,T_s}{J}e^{-\frac{c}{J}T_s} + e^{-\frac{c}{J}T_s} - 1\right]} = \frac{\lambda + e^{-\lambda} - 1}{\lambda e^{-\lambda} + e^{-\lambda} - 1}$$

$$z_{z_1} = \frac{\lambda + e^{-\lambda} - 1}{\lambda e^{-\lambda} + e^{-\lambda} - 1} \qquad \text{where} \quad \lambda = -\frac{cT_s}{J}$$

2.1.5 M220 - DC Brushless Motor

I. DC Brushless Motor Overview

The **DC brushless motor** is known also as *permanent magnet synchronous motor*.
The main advantage over the conventional *DC brush motor* is the elimination of brush friction associated wear. Other advantage is greater volume-to-power ratio.

The permanent magnets are fixed on the rotor. The three phase windings are distributed in slots of the stator.

In a DC brushless motor, a rotor positioning sensor is used and the commutation procedure is done electronically: it can be *rectangular* or *sinusoidal*.

A brushless dc motor is essentially a dc motor turned inside out. However, the basic principle of operation of a brushless dc motor is similar to that of a normal dc motor. A brushless dc motor has a rotor with permanent magnets and a stator with windings that are connected to the control electronics. The control electronics act as a replacement for the commutator and perform its function of energizing the proper winding. The windings are energized in a pattern which rotates around the stator. Then the energized stator winding leads to the rotor magnet and switches just as the rotor aligns with the stator. In contrast to the conventional dc motor, the permanent magnets of the brushless dc motor are affixed directly onto the rotor itself. The phase windings (there are typically 3 phases) are distributed in the slots found on the stator. This arrangement provides for greater heat dissipation, which in turn leads to improved life and typically greater volume-to-power ratios for brushless motors than for brush motors. In any continuously rotating motor, to provide a continuous torque, the current must be successively altered or switched depending on the absolute position of the rotor. In a dc brushless motor, a rotor-positioning (opto) sensor is used and the commutation procedure is performed electronically. A brushless dc motor is actually cleaner, faster, more efficient, less noisy, and more reliable than a brush motor because there are no sparks involved in a brushless dc motor, and because a brushless dc motor is not restricted by the limitations of brush life, brush residue, maximum speed, and electric noise. One advantage of the brushless dc motor is its ability to use opto sensors that can provide reliable position sensing in harsh environments where high vibration, moisture and relatively high temperatures exist and because they are also known for their long life, fast response time, high repeatability, and zero speed-sensing capabilities.

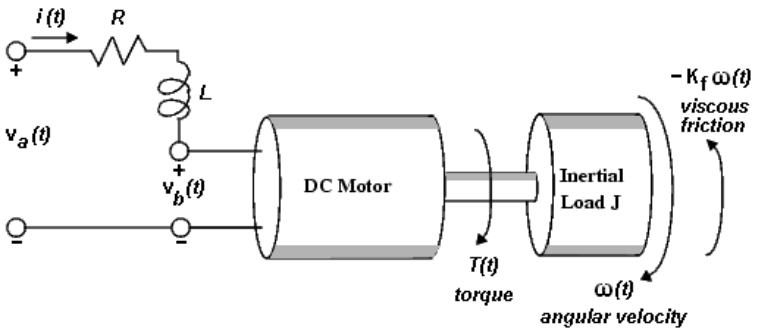

where

$\omega(t)$ - is the motor shaft angular velocity.
$T(t)$ - is the torque of the motor.
$v_a(t)$ - is the applied voltage.
$v_b(t)$ - is the back (induced) voltage.
K_b - is the motor constant.
K_t - is the motor torque constant (called also the motor armature constant).
K_f - is the motor viscous friction (damping), a function of motor's angular velocity.
L - is the armature winding inductance.
R - is the armature resistance.
J_m - is the motor's moment of inertia.

2. Electrical Equations

The torque $T(t)$ seen at the shaft of the motor is proportional to the current $i(t)$ induced by the applied voltage, $v_a(t)$,

$$T(t) = K_t\, i(t)$$

where K_t is the armature constant, is related to physical properties of the motor, such as magnetic field strength, the number of turns of wire around the conductor coil, and so on.

The back (induced) electromotive force, $v_b(t)$, is a voltage proportional to the angular velocity $\omega(t)$ seen at the motor shaft,

$$v_b(t) = K_b\, \omega(t)$$

where K_b, the motor constant, also depends on certain physical properties of the motor.

$$v_a(t) - v_b(t) = L\frac{di}{dt} + R\, i(t)$$

$$v_a(t) = L\frac{di}{dt} + R\, i(t) + K_b\, \omega(t)$$

$$\frac{di}{dt} = -\frac{R}{L}\, i(t) - \frac{K_b}{L}\, \omega(t) + \frac{1}{L}\, v_a(t)$$

II. Mechanical Equations

The mechanical part of the motor equations is derived using Newton's law, which states that the inertial load J_m times the derivative of angular rate (i.e. angular velocity) equals the sum of all the torques about the motor shaft.

$$J_m\, \frac{d\omega}{dt} = \sum T_i = -K_f\, \omega(t) + T(t)$$

$$T(t) = J_m\, \frac{d\omega}{dt} + K_f\, \omega(t)$$

$$J_m\, \frac{d\omega}{dt} = -K_f\, \omega(t) + K_m\, i(t)$$

where $-K_f\, \omega(t)$ is a linear approximation for viscous friction.

$$\frac{d\omega}{dt} = -\frac{K_f}{J_m}\, \omega(t) + \frac{K_m}{J_m}\, i(t)$$

III. State-Space Equations for the DC Brushless Motor

Given the two differential equations derived in the last section, we can now develop a state-space representation of the DC motor as a dynamic system. The current $i(t)$ and the angular velocity $\omega(t)$ are the two states of the system. The applied voltage, $v_a(t)$, is the input to the system, and the angular velocity $\omega(t)$ is the output.

$$\begin{cases} \dfrac{di}{dt} = -\dfrac{R}{L}\, i(t) - \dfrac{K_b}{L}\, \omega(t) + \dfrac{1}{L}\, v_a(t) \\ \dfrac{d\omega}{dt} = -\dfrac{K_f}{J_m}\, \omega(t) + \dfrac{K_m}{J_m}\, i(t) \end{cases}$$

IV. Block Diagrams

Diagram 1

Applying Laplace transform to the following equation

$$v_a(t) - v_b(t) = L\frac{di}{dt} + R\,i(t)$$

we have

$$V_a(s) - V_b(s) = sL\,I(s) + R\,I(s)$$

$$\frac{I(s)}{V_a(s) - V_b(s)} = \frac{1}{sL + R}$$

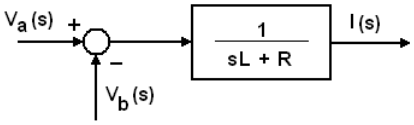

Diagram 2

From $$T(t) = K_t\,i(t)$$

we get

$$T(s) = K_t\,I(s)$$

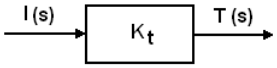

Diagram 3

In the same manner, applying Laplace to

$$T(t) = J_m\,\frac{d\omega}{dt} + K_f\,\omega(t)$$

it results

$$T(s) = J_m s\,\Omega(s) - K_f\,\Omega(s)$$

$$\frac{\Omega(s)}{T(s)} = \frac{1}{s\,J_m + K_f}$$

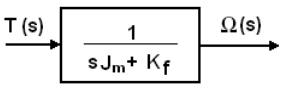

Diagram 4

From $$v_b(t) = K_b\,\omega(t)$$

we get

$$V_b(s) = K_b\,\Omega(s)$$

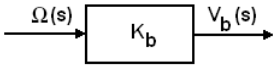

DC Motor Block Diagram

Connecting all the four block diagrams above we obtain the DC Motor block diagram.

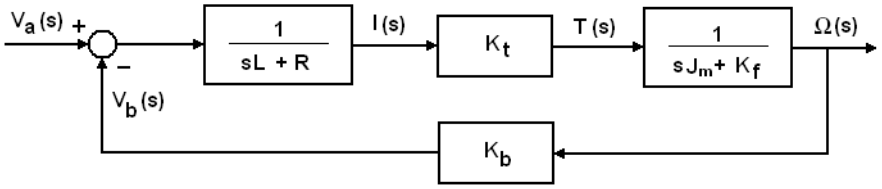

V. Transfer Functions

A. The transfer function between the applied voltage and the angular velocity of the shaft of the motor

From the above diagram block we can write the transfer function between the input of the motor, the applied voltage $V_a(s)$ and its output, the angular velocity of the shaft of the motor, $\Omega(s)$ as:

$$H_1(s) = \frac{\Omega(s)}{V_a(s)} = \frac{\dfrac{K_t}{(sL+R)}\dfrac{1}{(sJ_m+K_f)}}{1+K_b\dfrac{K_t}{(sL+R)}\dfrac{1}{(sJ_m+K_f)}} = \frac{K_t}{(sL+R)(sJ_m+K_f)+K_bK_t}$$

B. The transfer function between the applied voltage and the torque of the motor

The transfer function between the input of the motor, the applied voltage $V_a(s)$ and its output, the torque of the motor, $T(s)$ can be written modifying the last diagram block as follows.

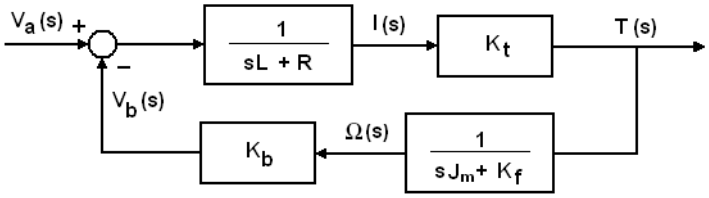

$$H_2(s) = \frac{T(s)}{V_a(s)} = \frac{\dfrac{K_t}{(sL+R)}}{1+K_b\dfrac{1}{(sJ_m+K_f)}\dfrac{K_t}{(sL+R)}} = \frac{K_t(sJ_m+K_f)}{(sL+R)(sJ_m+K_f)+K_bK_t} = \frac{order\ 1}{order\ 2}$$

$$H_2(s) = \frac{T(s)}{V_a(s)} = \frac{sK_tJ_m+K_tK_f}{s^2LJ_m+s(LK_f+RJ_m)+RK_f+K_bK_t} = \frac{s\dfrac{K_t}{L}+\dfrac{K_tK_f}{LJ_m}}{s^2+s\dfrac{LK_f+RJ_m}{LJ_m}+\dfrac{RK_f+K_bK_t}{LJ_m}}$$

2.1.6 Zero-order hold for DC motor and plant together

$$H(s) = H_m(s)\,H_p(s) = \frac{s\,\dfrac{K_t}{L} + \dfrac{K_t K_f}{L J_m}}{s^2 + s\,\dfrac{L K_f + R J_m}{L J_m} + \dfrac{R K_f + K_b K_t}{L J_m}} \; \frac{n_g}{J s^2 + c s} = \frac{s\,n_g \dfrac{K_t}{L} + n_g \dfrac{K_t K_f}{L J_m}}{s(J s + c)\left(s^2 + s\,\dfrac{L K_f + R J_m}{L J_m} + \dfrac{R K_f + K_b K_t}{L J_m}\right)}$$

Simplifying the notations

$$m_1 = n_g \frac{K_t}{L} \qquad m_2 = n_g \frac{K_t K_f}{L J_m}$$
$$n_1 = \frac{L K_f + R J_m}{L J_m} \qquad n_2 = \frac{R K_f + K_b K_t}{L J_m}$$

we have

$$H(s) = \frac{s\,m_1 + m_2}{s(J s + c)(s^2 + s\,n_1 + n_2)}$$

CASE 1 - The factor $s^2 + s\,n_1 + n_2$ has two complex conjugated roots

$$H(z) = (1 - z^{-1})\mathcal{Z}\left[\mathcal{L}^{-1}\left\{\frac{H(s)}{s}\right\}\right] = (1 - z^{-1})\mathcal{Z}\left[\mathcal{L}^{-1}\left\{\frac{\frac{s\,m_1 + m_2}{s(J s + c)(s^2 + s\,n_1 + n_2)}}{s}\right\}\right] = (1 - z^{-1})\mathcal{L}^{-1}\left\{\frac{s\,m_1 + m_2}{s^2(J s + c)(s^2 + s\,n_1 + n_2)}\right\}$$

$$\frac{s\,m_1 + m_2}{s^2(J s + c)(s^2 + s\,n_1 + n_2)} = \frac{A}{s^2} + \frac{B}{s} + \frac{C}{J s + c} + \frac{D s + E}{s^2 + s\,n_1 + n_2}$$

where

$$A = \frac{m_2}{c\,n_2}$$
$$B = \frac{m_1\,c\,n_2 - m_2\,(J\,n_2 + c\,n_1)}{c^2 {n_2}^2}$$
$$C = \frac{J^3\,(m_2 J - m_1\,c)}{c^2\left(J^2 n_2 - J\,c\,n_1 + c^2\right)}$$
$$D = \frac{m_1\,n_2\,(J n_1 - c\,) + m_2\left(c\,n_1 - J\left({n_1}^2 - n_2\right)\right)}{{n_2}^2(J^2 n_2 - J\,c\,n_1 + c^2)}$$
$$E = \frac{m_1\,n_2\left(J\left({n_1}^2 - n_2\right) - c\,n_1\right) - m_2\left(J n_1\left({n_1}^2 - 2 n_2\right) + c\left(n_2 - {n_1}^2\right)\right)}{{n_2}^2(J^2 n_2 - J\,c\,n_1 + c^2)}$$

So we have

$$H(z) = (1 - z^{-1})\mathcal{Z}\left[\mathcal{L}^{-1}\left\{\frac{s\,m_1 + m_2}{s^2(J s + c)(s^2 + s\,n_1 + n_2)}\right\}\right] = (1 - z^{-1})\mathcal{Z}\left[\mathcal{L}^{-1}\left\{\frac{A}{s^2} + \frac{B}{s} + \frac{C}{J s + c} + \frac{D s + E}{s^2 + s\,n_1 + n_2}\right\}\right]$$

From the table above we have

$$\mathcal{Z}\left[\mathcal{L}^{-1}\left\{\frac{A}{s^2}\right\}\right] = \frac{A\,T_s z}{(z-1)^2}$$
$$\mathcal{Z}\left[\mathcal{L}^{-1}\left\{\frac{B}{s}\right\}\right] = \frac{B z}{z-1}$$
$$\mathcal{Z}\left[\mathcal{L}^{-1}\left\{\frac{C}{J s + c}\right\}\right] = \frac{\dfrac{C}{J} z}{z - e^{-\frac{c}{J} T_s}}$$

Let us calculate

Laplace Domain	Time domain	Z Domain ($t=nT_s$)
1	$\delta(t)$ unit impulse	1
$\frac{1}{s}$	$u(t)$ unit step	$\frac{z}{z-1}$
$\frac{1}{s^2}$	t	$\frac{T_s z}{(z-1)^2}$
$\frac{1}{s+a}$	e^{-at}	$\frac{z}{z-e^{-aT_s}}$
$\frac{b}{(s+a)^2+b^2}$	$e^{-at}\sin(bt)$	$\frac{ze^{-aT_s}\sin(bT_s)}{z^2-2ze^{-aT_s}\cos(bT_s)+e^{-2aT_s}}$
$\frac{s+a}{(s+a)^2+b^2}$	$e^{-at}\cos(bt)$	$\frac{z^2-ze^{-aT_s}\cos(bT_s)}{z^2-2ze^{-aT_s}\cos(bT_s)+e^{-2aT_s}}$
$\frac{As+B}{s^2+2as+c}$	$e^{-at}\left[A\cos(bt)+\frac{B-aA}{b}\sin(bt)\right]$ $b=\sqrt{c-a^2}$	
$\frac{1}{(s-a)(s-b)}$ $a\neq b$	$\frac{e^{bt}-e^{at}}{b-a}$	
$\frac{s}{(s-a)(s-b)}$ $a\neq b$	$\frac{be^{bt}-ae^{at}}{b-a}$	

$$\mathcal{Z}\left[\mathcal{L}^{-1}\left\{\frac{Ds+E}{s^2+sn_1+n_2}\right\}\right]$$

$$\mathcal{L}^{-1}\left\{\frac{Ds+E}{s^2+sn_1+n_2}\right\}=e^{-\frac{n_1}{2}t}\left[D\cos(bt)+\frac{E-D\frac{n_1}{2}}{b}\sin(bt)\right]$$

$$\mathcal{Z}\left[e^{-\frac{n_1}{2}t}D\cos(bt)\right]=D\frac{z^2-ze^{-\frac{n_1}{2}T_s}\cos(bT_s)}{z^2-2ze^{-\frac{n_1}{2}T_s}\cos(bT_s)+e^{-2\frac{n_1}{2}T_s}}\qquad\text{where}\qquad b=\sqrt{n_2-\left(\frac{n_1}{2}\right)^2}$$

$$\mathcal{Z}\left[e^{-\frac{n_1}{2}t}\frac{E-D\frac{n_1}{2}}{b}\sin(bt)\right]=\frac{E-D\frac{n_1}{2}}{b}\frac{ze^{-\frac{n_1}{2}T_s}\sin(bT_s)}{z^2-2ze^{-\frac{n_1}{2}T_s}\cos(bT_s)+e^{-2\frac{n_1}{2}T_s}}\qquad\text{where}\qquad b=\sqrt{n_2-\left(\frac{n_1}{2}\right)^2}$$

$$\mathcal{Z}\left[\mathcal{L}^{-1}\left\{\frac{Ds+E}{s^2+sn_1+n_2}\right\}\right]=D\frac{z^2-ze^{-\frac{n_1}{2}T_s}\cos(bT_s)}{z^2-2ze^{-\frac{n_1}{2}T_s}\cos(bT_s)+e^{-2\frac{n_1}{2}T_s}}+\frac{E-D\frac{n_1}{2}}{b}\frac{ze^{-\frac{n_1}{2}T_s}\sin(bT_s)}{z^2-2ze^{-\frac{n_1}{2}T_s}\cos(bT_s)+e^{-2\frac{n_1}{2}T_s}}$$

$$\mathcal{Z}\left[\mathcal{L}^{-1}\left\{\frac{Ds+E}{s^2+sn_1+n_2}\right\}\right]=\frac{D\left(z^2-ze^{-\frac{n_1}{2}T_s}\cos(bT_s)\right)+\frac{E-D\frac{n_1}{2}}{b}ze^{-\frac{n_1}{2}T_s}\sin(bT_s)}{z^2-2ze^{-\frac{n_1}{2}T_s}\cos(bT_s)+e^{-2\frac{n_1}{2}T_s}}$$

$$\mathcal{Z}\left[\mathcal{L}^{-1}\left\{\frac{Ds+E}{s^2+sn_1+n_2}\right\}\right]=\frac{Dz^2-z\left(e^{-\frac{n_1}{2}T_s}\left[D\cos(bT_s)-\frac{E-D\frac{n_1}{2}}{b}\sin(bT_s)\right]\right)}{z^2-2ze^{-\frac{n_1}{2}T_s}\cos(bT_s)+e^{-2\frac{n_1}{2}T_s}}\qquad\text{where}\qquad b=\sqrt{n_2-\left(\frac{n_1}{2}\right)^2}$$

$$H(z)=(1-z^{-1})\left[\frac{AT_sz}{(z-1)^2}+\frac{Bz}{z-1}+\frac{\frac{C}{J}z}{z-e^{-\frac{c}{J}T_s}}+\frac{Dz^2-z\left(e^{-\frac{n_1}{2}T_s}\left[D\cos(bT_s)-\frac{E-D\frac{n_1}{2}}{b}\sin(bT_s)\right]\right)}{z^2-2ze^{-\frac{n_1}{2}T_s}\cos(bT_s)+e^{-2\frac{n_1}{2}T_s}}\right]$$

$$H(z)=\frac{\cancel{z-1}}{\cancel{z}}\left[\frac{AT_s\cancel{z}}{(z-1)\cancel{z}}+\frac{B\cancel{z}}{\cancel{z-1}}+(z-1)\frac{\frac{C}{J}\cancel{z}}{z-e^{-\frac{c}{J}T_s}}+(z-1)\frac{Dz\cancel{z}-z\left(e^{-\frac{n_1}{2}T_s}\left[D\cos(bT_s)-\frac{E-D\frac{n_1}{2}}{b}\sin(bT_s)\right]\right)}{z^2-2ze^{-\frac{n_1}{2}T_s}\cos(bT_s)+e^{-2\frac{n_1}{2}T_s}}\right]$$

$$H(z)=\frac{AT_s}{z-1}+B+(z-1)\frac{\frac{C}{J}}{z-e^{-\frac{c}{J}T_s}}+(z-1)\frac{Dz-\left(e^{-\frac{n_1}{2}T_s}\left[D\cos(bT_s)-\frac{E-D\frac{n_1}{2}}{b}\sin(bT_s)\right]\right)}{z^2-2ze^{-\frac{n_1}{2}T_s}\cos(bT_s)+e^{-2\frac{n_1}{2}T_s}}$$

where $\quad b=\sqrt{n_2-\left(\frac{n_1}{2}\right)^2}$

Using the notations below, we can rewrite:

$$H(z)=\frac{AT_s}{z-1}+B+(z-1)\frac{\frac{C}{J}}{z+\alpha}+(z-1)\frac{Dz+\beta}{z^2+\gamma z+\delta}$$

where

$$\begin{aligned}\alpha&=-e^{-\frac{c}{J}T_s}\\ \beta&=-\left(e^{-\frac{n_1}{2}T_s}\left[D\cos(bT_s)-\frac{E-D\frac{n_1}{2}}{b}\sin(bT_s)\right]\right)\\ \gamma&=-2e^{-\frac{n_1}{2}T_s}\cos(bT_s)\\ \delta&=e^{-2\frac{n_1}{2}T_s}\end{aligned}$$

$$H(z)=\frac{AT_s(z+\alpha)(z^2+\gamma z+\delta)+B(z-1)(z+\alpha)(z^2+\gamma z+\delta)+\frac{C}{J}(z-1)^2(z^2+\gamma z+\delta)+(Dz+\beta)(z-1)^2(z+\alpha)}{(z-1)(z+\alpha)(z^2+\gamma z+\delta)}$$

$$H(z)=\frac{z^4(B+\frac{C}{J}+D)+z^3(AT_s+B(\alpha+\gamma-1)+\frac{C}{J}(\gamma-2)+D(\alpha-2)+\beta)+}{z^4+z^3(\alpha+\gamma-1)+z^2(\alpha(\gamma-1)-\gamma+\delta)-z(\alpha(\gamma-\delta)+\delta)-\alpha\delta}$$

$$\frac{+z^2(AT_s(\alpha+\gamma)+B(\alpha(\gamma-1)-\gamma+\delta)-\frac{C}{J}(2\gamma-\delta-1)+D(1-2\alpha)+\beta(\alpha-2))+}{z^4+z^3(\alpha+\gamma-1)+z^2(\alpha(\gamma-1)-\gamma+\delta)-z(\alpha(\gamma-\delta)+\delta)-\alpha\delta}$$

$$\frac{+z(AT_s(\alpha\gamma+\delta)-B(\alpha(\gamma-\delta)+\delta)+\frac{C}{J}(\gamma-2\delta)+D\alpha-\beta(2\alpha-1))+}{z^4+z^3(\alpha+\gamma-1)+z^2(\alpha(\gamma-1)-\gamma+\delta)-z(\alpha(\gamma-\delta)+\delta)-\alpha\delta}$$
$$\frac{+AT_s\alpha\delta-B\alpha\delta+\frac{C}{J}\delta+\alpha\beta}{z^4+z^3(\alpha+\gamma-1)+z^2(\alpha(\gamma-1)-\gamma+\delta)-z(\alpha(\gamma-\delta)+\delta)-\alpha\delta}$$

$$H(z)=\frac{b_1z^4+b_2z^3+b_3z^2+b_4z+b_5}{z^4+a_1z^3+a_2z^2+a_3z+a_4}=\frac{order\ 4}{order\ 4}$$

where

$$b_1=B+\frac{C}{J}+D$$
$$b_2=AT_s+B(\alpha+\gamma-1)+\frac{C}{J}(\gamma-2)+D(\alpha-2)+\beta$$
$$b_3=AT_s(\alpha+\gamma)+B(\alpha(\gamma-1)-\gamma+\delta)-\frac{C}{J}(2\gamma-\delta-1)+D(1-2\alpha)+\beta(\alpha-2)$$
$$b_4=AT_s(\alpha\gamma+\delta)-B(\alpha(\gamma-\delta)+\delta)+\frac{C}{J}(\gamma-2\delta)+D\alpha-\beta(2\alpha-1)$$
$$b_5=AT_s\alpha\delta-B\alpha\delta+\frac{C}{J}\delta+\alpha\beta$$

$$a_1=\alpha+\gamma-1$$
$$a_2=\alpha(\gamma-1)-\gamma+\delta$$
$$a_3=-(\alpha(\gamma-\delta)+\delta)$$
$$a_4=-\alpha\delta$$

CASE 2 - The factor $s^2+sn_1+n_2$ has two real roots

$$H(z)=(1-z^{-1})\mathcal{Z}\left[\mathcal{L}^{-1}\left\{\frac{H(s)}{s}\right\}\right]=(1-z^{-1})\mathcal{Z}\left[\mathcal{L}^{-1}\left\{\frac{\frac{sm_1+m_2}{s(Js+c)(s-a)(s-b)}}{s}\right\}\right]=(1-z^{-1})\mathcal{L}^{-1}\left\{\frac{sm_1+m_2}{s^2(Js+c)(s-a)(s-b)}\right\}$$
$$\frac{sm_1+m_2}{s^2(Js+c)(s-a)(s-b)}=\frac{A}{s^2}+\frac{B}{s}+\frac{C}{Js+c}+\frac{D}{s-a}+\frac{E}{s-b}$$

where

$$a=\frac{-n_1+\sqrt{{n_1}^2-4n_2}}{2}\qquad\text{and}\qquad b=\frac{-n_1-\sqrt{{n_1}^2-4n_2}}{2}$$

$$A=\frac{m_2}{abc}$$
$$B=\frac{a(b(cm_1-Jm_2)+cm_2)+bcm_2}{a^2b^2c^2}$$
$$C=\frac{J^3(Jm_2-cm_1)}{c^2(aJ+c)(bJ+c)}$$
$$D=\frac{am_1+m_2}{a^2(a-b)(aJ+c)}$$

$$E = \frac{bm_1 + m_2}{b^2(b-a)(bJ+c)}$$

$$H(z) = (1-z^{-1})\mathcal{Z}\left[\mathcal{L}^{-1}\left\{\frac{sm_1+m_2}{s^2(Js+c)(s-a)(s-b)}\right\}\right] = (1-z^{-1})\mathcal{Z}\left[\mathcal{L}^{-1}\left\{\frac{A}{s^2}+\frac{B}{s}+\frac{C}{Js+c}+\frac{D}{s-a}+\frac{E}{s-b}\right\}\right]$$

From the Laplace table we have

$$\mathcal{Z}\left[\mathcal{L}^{-1}\left\{\frac{A}{s^2}\right\}\right] = \frac{AT_s z}{(z-1)^2}$$

$$\mathcal{Z}\left[\mathcal{L}^{-1}\left\{\frac{B}{s}\right\}\right] = \frac{Bz}{z-1}$$

$$\mathcal{Z}\left[\mathcal{L}^{-1}\left\{\frac{C}{Js+c}\right\}\right] = \frac{\frac{C}{J}z}{z-e^{-\frac{c}{J}T_s}}$$

$$\mathcal{Z}\left[\mathcal{L}^{-1}\left\{\frac{D}{s-a}\right\}\right] = \frac{Dz}{z-e^{aT_s}}$$

$$\mathcal{Z}\left[\mathcal{L}^{-1}\left\{\frac{E}{s-b}\right\}\right] = \frac{Ez}{z-e^{bT_s}}$$

$$H(z) = \frac{z-1}{z}\left[\frac{AT_s z}{(z-1)^2}+\frac{Bz}{z-1}+\frac{\frac{C}{J}z}{z-e^{-\frac{c}{J}T_s}}+\frac{Dz}{z-e^{aT_s}}+\frac{Ez}{z-e^{bT_s}}\right]$$

$$H(z) = \frac{AT_s}{z-1}+B+\frac{\frac{C}{J}(z-1)}{z-e^{-\frac{c}{J}T_s}}+\frac{D(z-1)}{z-e^{aT_s}}+\frac{E(z-1)}{z-e^{bT_s}}$$

$$H(z) = \frac{(AT_s)(z+\alpha)(z+\beta)(z+\gamma)+B(z-1)(z+\alpha)(z+\beta)(z+\gamma)+\frac{C}{J}(z-1)^2(z+\beta)(z+\gamma)+}{(z-1)(z+\alpha)(z+\beta)(z+\gamma)}$$

$$\frac{+D(z-1)^2(z+\alpha)(z+\gamma)+E(z-1)^2(z+\alpha)(z+\beta)}{(z-1)(z+\alpha)(z+\beta)(z+\gamma)}$$

where

$$\alpha = -e^{-\frac{c}{J}T_s}$$

$$\beta = -e^{aT_s}$$

$$\gamma = -e^{bT_s}$$

$$H(z) = \frac{z^4(B+\frac{C}{J}+D+E)+z^3(AT_s+B(\alpha+\beta+\gamma-1)+\frac{C}{J}(\beta+\gamma-2))+D(\alpha+\gamma-2)+E(\alpha+\beta-2)+}{z^4+z^3(\alpha+\beta+\gamma-1)+z^2(\alpha(\beta+\gamma-1)+\beta(\gamma-1)-\gamma)+z(\alpha(\beta(\gamma-1)-\gamma)-\beta\gamma)-\alpha\beta\gamma}$$

$$\frac{+z^2(AT_s(\alpha+\beta+\gamma)+B(\alpha(\beta+\gamma-1)+\beta(\gamma-1)-\gamma)+\frac{C}{J}(\beta(\gamma-2)-2\gamma+1))+D(\alpha(\gamma-2)-2\gamma+1)+E(\alpha(\beta-2)-2\beta+1)+}{z^4+z^3(\alpha+\beta+\gamma-1)+z^2(\alpha(\beta+\gamma-1)+\beta(\gamma-1)-\gamma)+z(\alpha(\beta(\gamma-1)-\gamma)-\beta\gamma)-\alpha\beta\gamma}$$

$$\frac{+z(AT_s(\alpha(\beta+\gamma)+\beta\gamma)+B(\alpha(\beta(\gamma-1)-\gamma)-\beta\gamma)+\frac{C}{J}(\gamma-\beta(2\gamma-1)))+D(\gamma-\alpha(2\gamma-1))+E(\beta-\alpha(2\beta-1))+}{z^4+z^3(\alpha+\beta+\gamma-1)+z^2(\alpha(\beta+\gamma-1)+\beta(\gamma-1)-\gamma)+z(\alpha(\beta(\gamma-1)-\gamma)-\beta\gamma)-\alpha\beta\gamma}$$

$$\frac{+AT_s\alpha\beta\gamma - B\alpha\beta\gamma + \frac{C}{J}\beta\gamma + D\alpha\gamma + E\alpha\beta}{z^4 + z^3(\alpha+\beta+\gamma-1) + z^2(\alpha(\beta+\gamma-1)+\beta(\gamma-1)-\gamma) + z(\alpha(\beta(\gamma-1)-\gamma)-\beta\gamma) - \alpha\beta\gamma}$$

$$H(z) = \frac{b_1 z^4 + b_2 z^3 + b_3 z^2 + b_4 z + b_5}{z^4 + a_1 z^3 + a_2 z^2 + a_3 z + a_4} = \frac{order\ 4}{order\ 4}$$

where

$$b_1 = B + \frac{C}{J} + D + E$$

$$b_2 = AT_s + B(\alpha+\beta+\gamma-1) + \frac{C}{J}(\beta+\gamma-2) + D(\alpha+\gamma-2) + E(\alpha+\beta-2)$$

$$b_3 = AT_s(\alpha+\beta+\gamma) + B(\alpha(\beta+\gamma-1)+\beta(\gamma-1)-\gamma) + \frac{C}{J}(\beta(\gamma-2)-2\gamma+1) + D(\alpha(\gamma-2)-2\gamma+1) + E(\alpha(\beta-2)-2\beta+1)$$

$$b_4 = (AT_s(\alpha(\beta+\gamma)+\beta\gamma) + B(\alpha(\beta(\gamma-1)-\gamma)-\beta\gamma) + \frac{C}{J}(\gamma-\beta(2\gamma-1)) + D(\gamma-\alpha(2\gamma-1)) + E(\beta-\alpha(2\beta-1))$$

$$b_5 = AT_s\alpha\beta\gamma - B\alpha\beta\gamma + \frac{C}{J}\beta\gamma + D\alpha\gamma + E\alpha\beta$$

$$a_1 = \alpha+\beta+\gamma-1$$

$$a_2 = \alpha(\beta+\gamma-1)+\beta(\gamma-1)-\gamma$$

$$a_3 = \alpha(\beta(\gamma-1)-\gamma)-\beta\gamma$$

$$a_4 = -\alpha\beta\gamma$$

CASE 3 - The motor is considered as being only a constant k_M

$$H_m(s) = \frac{s\frac{K_t}{L} + \frac{K_t K_f}{LJ_m}}{s^2 + s\frac{LK_f + RJ_m}{LJ_m} + \frac{RK_f + K_b K_t}{LJ_m}} = k_M$$

And therefore the plant becomes:

$$H(s) = \frac{n_g\, k_M}{s(Js+c)}$$

2.2 STEP RESPONSE IDENTIFICATION

The plant transfer function we use is: $\frac{n_g k_M}{s(Js+c)}$

It can be rewritten as: $\frac{k}{s(s+a)}$ where $k = \frac{n_g k_M}{J}$ and $a = \frac{c}{J}$

The step response is: $\frac{vk}{s^2(s+a)} = \frac{\alpha_1}{s^2} + \frac{\alpha_2}{s} + \frac{\alpha_3}{s+a}$

where

$$\alpha_1 = \frac{kv}{a}$$

$$\alpha_2 = -\frac{kv}{a^2}$$

$$\alpha_3 = \frac{kv}{a^2}$$

$$v = 0.25\,(volts)$$

The time response of the transfer function above is: $\theta = \alpha_1 t + \alpha_2 + \alpha_3 e^{-a_1 t}$

We perform a step input of 0.25 volts and we measure the output.

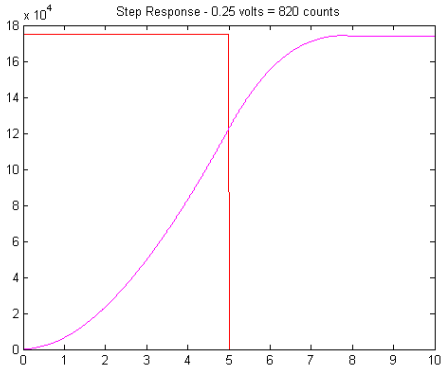

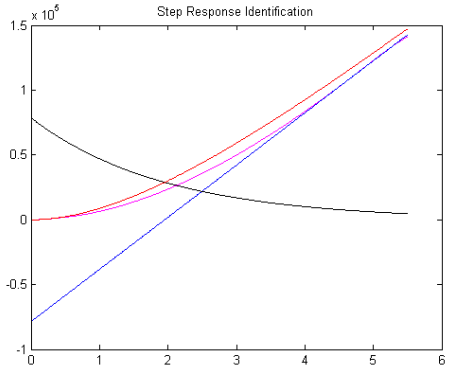

Considering two well-chosen points: $t_1 = 4.44\,(sec)$, $y_1 = 100080\,(counts)$ and $t_2 = 4.91\,(sec)$, $y_2 = 118992\,(counts)$

We can calculate the straight line approximation $\theta = \alpha_1 t + \alpha_2$.
and obtain:

$$\alpha_1 = 40238.299$$

$$\alpha_2 = -78578.042$$

With the above values we can calculate all the other parameters:

$$\alpha_3 = -\alpha_2 = 78578.042$$

$$a = -\frac{\alpha_1}{\alpha_2} = 0.512081$$

$$k = \frac{\alpha_1\, a}{v} = \frac{40238.299 * 0.512081}{0.25} = 82421.020583$$

The plant seen by software is:
Therefore

$$\frac{\theta_{software}}{u_{software}} = k_c \frac{n_g k_M}{s(Js+c)} = \frac{k'}{s(s+a)}$$

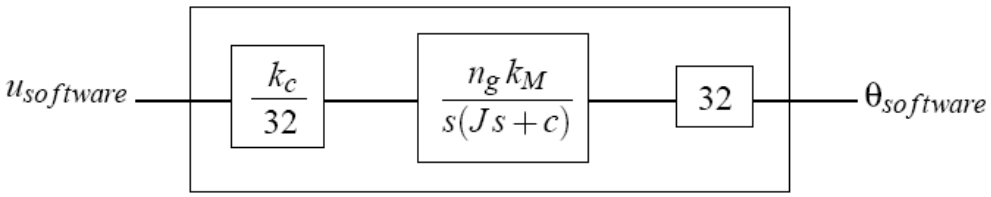

where

$$k_c = \frac{10}{32,762}\,(V/counts) = 0.000305231\,(V/counts)$$

$$k = 82421.020583$$

$$a = 0.512081$$

$$k' = k_c\,k = 0.000305231 * 82421.020583 = 25.1575058$$

The identified plant is then:

$$H(s) = k_c\,\frac{n_g\,k_M}{s(Js+c)} = \frac{k'}{s(s+a)} = \frac{25.1575058}{s(s+0.512081)}$$

Based on the values obtained, we can calculate the PI controller parameters (k_p and T_i) for velocity control of the closed-loop system as follows:

$$k_p = \frac{1}{k'} = 0.0397496 \qquad \text{and} \qquad T_i = \frac{1}{a} = 1.9528173$$

The conversion table for the M220 plant is:

count	**volt**	**degree**	**radian**
1	0.000304879909	0.0225	0.0003927
3279.979987	1	73.7995497	1.2880481
44.44444	0.01355	1	0.0174533
2546.47881	0.776358	57.295779	1

2.3 COULOMB AND VISCOUS FRICTION IDENTIFICATION

To obtain the Coulomb and viscous frictional coefficients we perform, as suggested in [22], steady-state experiments under closed-loop PI velocity control. We carry through the experiment with the PI parameters obtained in the previous section for velocities in the range of $150 - 40000$ counts/sec or approximately $0.05 - 15.7$ rad/sec in both directions of motion. We measure the control signal in each of those instances using high-quality sensors. At small velocities the data is of poor quality due especially to the stick-slip motion phenomenon. The nonlinear relationship between control signal (which represents the *friction force*) and velocity can be easily noted. There must be indicated that there has been observed a small steady-state error in the PI velocity control and also a small limit cycle, facts noted in the literature as occurring in such type of experiments.

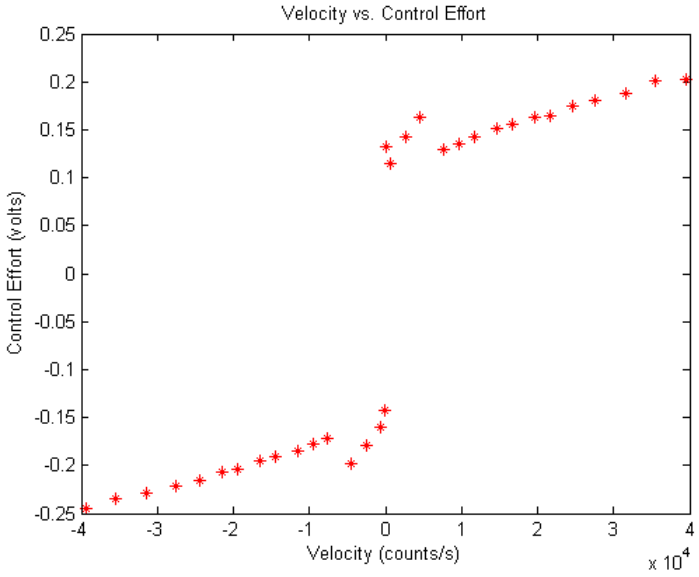

The raw data obtained is:

Control up	Velocity up	Control down	Velocity down
0.13291	158.61993	-0.14306	-131.97614
0.11534	704.68326	-0.15937	-590.80878
0.14277	2637.28385	-0.17850	-2544.77089
0.16287	4588.6473	-0.19833	-4496.91078
0.13006	7677.99788	-0.17119	-7571.57481
0.13586	9666.24951	-0.17769	-9558.1182
0.14242	11652.54720	-0.18464	-11543.3784
0.15192	14632.93197	-0.19133	-14530.96098
0.15529	16627.40154	-0.19537	-16523.79769
0.16253	19613.57036	-0.20336	-19508.016682
0.16513	21610.05688	-0.20703	-21501.80729
0.17404	24591.94361	-0.21588	-24483.82779
0.18018	27580.91909	-0.22185	-27473.34732
0.18855	31565.72812	-0.22920	-31460.84426
0.20073	35540.79387	-0.23521	-35451.76198
0.20307	39541.20573	-0.24493	-39433.13802

Using the data, the two direction-dependent viscous friction coefficients have been obtained by first degree polynomial curve fitting of the data, the points of higher velocities especially, in a least squares sense. This gives the straight line approximation which represents the *viscous* friction force. At the intersection of the line with the vertical zero velocity axis we obtain the two direction-dependent *Coulomb* friction coefficients.

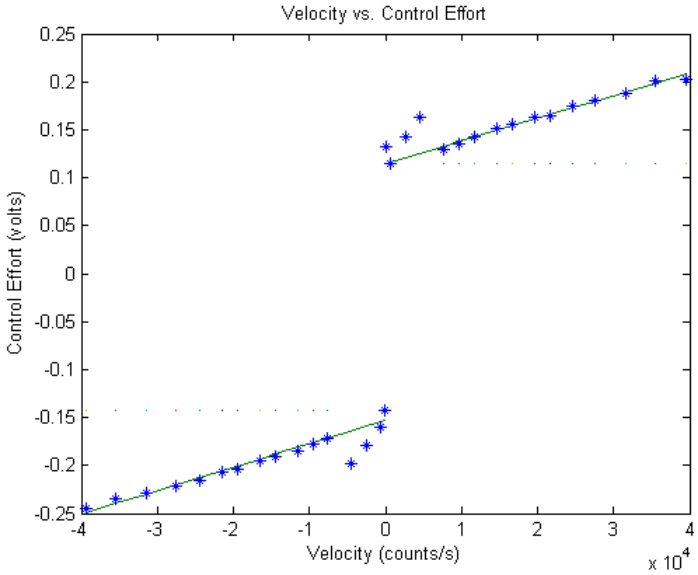

For the upper straight line $y_{up} = m_1 x + b_1$

- the slope is $m_1 = 2.3517 * 10^{-6}$
- the y-intercept is $b_1 = 0.114716$

The lower straight line $y_{down} = m_2 x + b_2$

- the slope is $m_2 = 2.4484 * 10^{-6}$
- the y-intercept is $b_2 = -0.152784.$

Coulomb friction component is: $F = F_C \, sgn(v)$

Viscous friction component is: $F = F_v \, v$

$F_C^+ = 0.114716$ (volts)

$F_v^+ = 2.3517 * 10^{-6}$ (volts·sec/counts)

$F_C^- = -0.152784$ (volts)

$F_v^- = 2.4484 * 10^{-6}$ (volts·sec/counts)

2.4 REFERENCES

[1] Blau, P.J., *Friction Science and Technology*, L.L. Faulkner (ed.), Marcel Dekker, Inc., New York, 1996.

[2] Armstrong-Hétlouvry B., P. Dupont, and C. Canudas de Wit, *A survey of models, analysis tools and compensation methods for the control of machines with friction*, Automatica, 30, 7, pp. 1083-1138, 1994.

[3] Canudas de Wit, C. H. Olsson, K. J. Åström, and P. Lischinsky, *A new model for control systems with friction*, IEEE Transactions on Automatic Control, AC-40, pp. 419-425, 1995.

[4] Haessig, Jr. D.A., and Friedland, B., *On the Modeling and Simulation of Friction*, Journal of Dynamic Systems, Measurements, and Control, 113, pp. 354-362, 1991.

[5] Bliman, P. A., and Sorine, M., *Easy-to-use Realistic Dry Friction Models for Automatic Control*, In Proc. of 3rd European Control Conference, Rome, Italy, pp. 3788-3794, 1995.

[6] Amontons, G., *De le résistance causée dans les machines*, Mémoires de l'Academie des Sciences, pp. 203-222, 1699.

[7] Coulomb, C.A., *Théorie des machines simples*, Mémoires de Mathématique et de Physique de l'Academie de Sciences, pp. 161-331, 1785.

[8] Stribeck, R., *Die Wesentlichen Eigenschaften der Gleit - und Rollenlager - the key qualities of sliding and roller bearings*, Zeitschrift des Vereines Seutscher Ingenieure, 46, 38, pp. 1342-48, 46, 39, 1432-1437, 1902.

[9] Johnson C. T. and Lorenz R. D., *Experimental identification of friction and its compensation in precise, position controlled mechanisms*, IEEE Transactions on Industry Applications, 28, 6, pp. 1392-1398, 1992.

[10] Rabinowicz E., *The nature of the static and kinetic coefficients of friction*, Journal of Applied Physics, 22, 11, 1373-1379, 1951.

[11] Armstrong-Hétlouvry B., *Stick slip and control in low-speed motion.* IEEE Transactions on Automatic Control, 38, 10, pp. 1483-1496, 1993.

[12] Armstrong-Hétlouvry B., *Control of Machines with Friction*, Kluwer Academic Publishers, Boston, Ma., 1991.

[13] Karnopp D., *Computer simulation of slip-stick friction in mechanical dynamic systems*, Journal of Dynamic Systems, Measurement, and Control, 107, 1, pp. 100-103, 1985.

[14] Olsson, H., Åström, K.J., Canudas de Wit, C., Gäfvert, M., and Lischinsky, P., *Friction Models and Friction Compensation*, European Journal of Control, 4, 3, pp. 176-195, 1998.

[15] Eborn, J., and Olsson, M., *Modelling and simulation of an industrial control loop with friction*, Proc. of the 4th IEEE Conference on Control Applications, Albany, New York, pp. 316-322, 1995.

[16] Courtney-Pratt, J., and Eisner, E., *The effect of a tangential force on the contact of metallic bodies*, In Proceedings of Royal Society, vol. A238, pp. 529-550, 1957.

[17] Hess, D.P., and Soom, A., *Friction at a lubricated line contact operating at oscillating sliding velocities*, Journal of Tribology, Vol. 112, pp. 147-152, 1990.

[18] Dahl P. R., *A solid friction model*, The Aerospace Corporation, El-Secundo, TOR-158(3107-18), California, 1968.

[19] Dupont P., Armstrong B., and Hayward V., *Elasto-plastic friction model: contact compliance and stiction*, In Proc. of American Control Conference, Vol. 2, 1072 - 1077, 2000.

[20] Harnoy A. and Friedland B., *Dynamic friction model of lubricated surfaces for precise motion control*, In Preprint No. 93-TC-1D-2. Society of Tribologists and Lubrication Engineers, 1993.

[21] Magnus Gäfvert - *Comparison of two Friction Models*, Master's thesis, LUTFD2/TFRT-5561-SE, Lund Institute Technology, Lund, Sweden, 1996.

[22] Magnus Gäfvert, *Comparisons of Two Dynamic Friction Models, Proc. of the 6th IEEE Conference on Control Applications*, Hartford, pp. 386-391, 1997.

[23] Barabanov N., and Ortega R., *Necessary and sufficient conditions for passivity of the LuGre friction model*, IEEE Transactions on Automatic Control, 45, 4, pp. 830-832, 2000.

[24] Swevers J., Al-Bender F., Ganseman C., and Prajogo T., *An integrated friction model structure with improved presliding behavior for accurate friction compensation*, IEEE Transactions on Automatic Control, 45, pp. 675-686, 2000.

[25] Ferretti G., Magnani. G., Manucci. G., Racco P., and Stampacchia V., *Friction model validation in sliding and presliding regimes with high resolution encoders*, in Experimental Robotics VIII, ser. STAR, Siciliano B. and Dario, Springer., pp. 328-337, 2003.

[26] Dupont P., Hayward V., Armstrong B., and Altpeter F., *Single state elastoplastic friction models*, IEEE Transactions on Automatic Control, 47, 12, pp. 787-792, 2002.

[27] Lampaert V., Swevers J., and Al-Bender F., *Modification of the Leuven Integrated Friction Model Structure*, IEEE Transactions on Automatic Control, 47, 4, pp. 683-687, 2002.

[28] Manual for Model 220 Industrial Emulator/Servo Trainer, Educational Control Products, CA 91367, 1995.